Title

Analytical characterization of laser induced plasmas towards uranium isotopic analysis in gaseous uranium hexafluoride

Authors

Chan, George C-Y
Martin, Leigh R
Trowbridge, Lee D
et al.

Publication Date

2021-02-01

DOI

10.1016/j.sab.2020.106036

Peer reviewed

Analytical Characterization of Laser Induced Plasmas towards Uranium Isotopic Analysis in Gaseous Uranium Hexafluoride

George C.-Y. Chan[a,*], Leigh R. Martin[b], Lee D. Trowbridge[b], Zhenli Zhu[a, c], Xianglei Mao[a], and Richard E. Russo[a, d,*]

[a] Lawrence Berkeley National Laboratory, Berkeley, CA 94720, USA

[b] Oak Ridge National Laboratory, Oak Ridge, TN 37830, USA

[c] State Key Laboratory of Biogeology and Environmental Geology, China University of Geosciences, Wuhan 430074, China

[d] Applied Spectra, 950 Riverside Pkwy Suite 90, West Sacramento, CA 95605, USA

(for submission to *Spectrochimica Acta Part B: Atomic Spectroscopy*)

*corresponding authors, email: gcchan@lbl.gov (G. Chan) and rerusso@lbl.gov (R.E. Russo)

Abstract

To perform direct enrichment assay on gaseous uranium hexafluoride (UF_6) with laser induced breakdown spectroscopy (LIBS), the dominant spectral-line features, evolution of the signal and background of the U II 424.437 nm line, and its Stark width and shift, were studied as a function of UF_6 gas pressure and pulse energy of a nanosecond Nd:YAG laser. Vapor pressure of UF_6 was found to be the most important parameter for LIBS analysis of gaseous UF_6. Spectral congestion with numerous U lines of high excitation potential was observed and signal-to-background ratio (SBR) was low for measurements with 80 torr UF_6. Only when both UF_6 vapor pressure and laser pulse energy were low, for example, less than 20 torr pressure and 30 mJ pulse energy, the resultant LIBS spectra from gaseous UF_6 resembled those obtained from solid U samples. The experimental data also suggest that U and F atoms recombine back to UF_6 after the laser pulse. The U emission was found decay fast with a persistent background signal, degrading SBR with delay time. Systematic positive biases were found for UF_6 enrichment assays performed with the ^{235}U–^{238}U line pair at 424.412–424.437 nm, which was confirmed to be caused by self-absorption. Even with optimization of experimental parameters and incorporation of a self-absorption term into the spectral-fitting algorithm, to reduce and compensate for self-absorption, self-absorption is still a main factor limiting accurate UF_6 enrichment assay. The use of another spectral window which contains no resonance line is a prospective solution for the self-absorption issue.

Keywords: Uranium hexafluoride; Enrichment assay; Isotopic analysis; Isotopic shift; LIBS

1. Introduction

Within the chemical analysis community, on-site measurement with fieldable instrumentation is one direction under concerted development [1-3]. In the area of analytical atomic spectrometry for inorganic elemental analysis where portable commercial instruments are available, laser induced breakdown spectroscopy (LIBS) and X-ray fluorescence (XRF), are the two most commonly used in-field techniques [1, 3-5]. LIBS and XRF share some similarities but also offer different capabilities; the two techniques are complementary. For instance, XFR is non-destructive whereas LIBS, although nominally destructive offers the option of standoff analysis, depth profiling of the sample, and significantly, the analysis of isotopes.

Although it is still largely in the development stage, optical emission from laser induced plasma (LIBS and a very similar technique termed LAMIS – laser ablation molecular isotopic spectrometry, which is based on molecular, instead of atomic, emission from a laser induced plasma) offers the feasibility for isotopic analysis, which is one area that LIBS is superior to XRF [4, 6]. Recent advances include: isotopic analyses of U with atomic emission [7, 8] and Li with self-reversal lines [9]; isotopic analyses of boron with the diatomic BO emission and multivariate calibration [10] and with the triatomic BO_2 molecular bands [11]; and comparison of hydrogen isotopic analysis with OH–OD and NH–ND molecular emission bands for liquid and frozen water samples [12]. In addition, a review on laser-induced plasma for standoff isotopic analysis [13] was recently published.

An analytical method for uranium isotopic analysis with LIBS was recently developed by our group [8]. Isotopic information of the solid sample (U_3O_8–$Li_2B_4O_7$ fused glassy disks) was

extracted from the LIBS spectra through multivariate nonlinear spectral fitting, which is theoretical in basis and does not require calibration with isotopically enriched standards. In brief, a spectral-line database consisting of twelve emission-line pairs with the corresponding isotopic shifts was built. The spectral-line database covers a relatively narrow spectral window from 424.300 to 424.500 nm. The experimentally measured LIBS spectra were fitted against this theoretical spectral-line database with the unknown ^{235}U isotopic content of the sample as one of the fitting parameters. The method was tested with a set of U-bearing glassy disks with ^{235}U enrichment ranging from natural (0.72%) to highly enriched levels (~93.2%), with results cross-validated with those obtained by thermal ionization mass spectrometry (TIMS) [8]. The analytical accuracies (biases) and precision in absolute [$^{235}U / (^{235}U + ^{238}U)$] ratios were about ±1% and 0.2%, respectively, and compare favorably with radiometric, non-destructive techniques (e.g., gamma spectroscopy).

Although LIBS is most commonly used for solid analysis, it can be applied to samples of any physical forms including liquid and gas. The objective of the present work is to test the feasibility of extending the application domain of the previously developed method [8] to a direct measurement of gaseous uranium hexafluoride (UF_6). Uranium hexafluoride is a white solid at room temperature but with very high vapor pressure (~80 torr [14]) and is the only known volatile compound of uranium [15]. Its low sublimation temperature together with the fact that fluorine has only a single naturally occurring isotope (so any difference in the molecular weight of UF_6 isotopologues must be from the different uranium isotopes [15]) makes UF_6 arguably the most important uranium compound involved in the uranium enrichment process. As the first line of defense against proliferation, accurate determinations of the uranium isotopic ratio (or enrichment) in UF_6 are critical for materials verification, accounting and safeguards. Currently,

mass spectrometry (MS) is the most sensitive measurement technique for the analysis of stable and long-lived isotopes. However, current MS techniques require too much infrastructure and operator expertise for field deployment and operation. Furthermore, shipping gaseous UF_6 samples off-site for MS-analysis is cumbersome, costly, and the results are not available for some time (months). In general, LIBS allows rapid, in-field analysis with near real-time results. Accordingly, LIBS is becoming increasingly popular for the analysis of special nuclear materials [7, 13, 16-18].

The present work is a first attempt, to our knowledge, to apply LIBS directly to gaseous UF_6 for enrichment assay. Here, we limit ourselves to direct UF_6 analysis without the use of a buffer gas because this method is designed for field (e.g., inside an enrichment plant) analysis. For field analysis, not only the method and the instrument hardware need to be as simple as possible, but also the requirements of consumables and procedures. Although the use of a buffer gas allows one to better tailor the plasma behavior and characteristics [19, 20], consumables (compressed gas) and procedures (particularly safety ones to avoid chamber overpressure with the introduced buffer gas) unavoidably complicate the process. Potentially, the method described in this paper greatly simplifies the procedures (only sampling without any sample preparation) and shortens the response time (on-site analysis, measurement within minutes) required for an UF_6 safeguards inspection.

As the characteristics of a laser induced plasma formed directly in gaseous UF_6 is almost an unexplored territory, we first performed fundamental characterization of the plasma, for example, the change of signal, background, Stark width and spectral shift with time, laser pulse energy, and UF_6 pressure. As will be discussed in subsequent sections, there is a fundamental

difference in the evolution of the laser induced plasma formed with solid U-bearing samples and breakdown directly in gaseous UF_6. The difference is significant so that the same spectral window from 424.300 to 424.500 nm, which showed success when applied to solid sample, is inadequate for gaseous UF_6 samples, primarily because of severe self-absorption.

2. Experimental

The experimental hardware was identical to that previously described [8], with two modifications as noted below. Figure 1 shows a photograph of the experimental setup. Briefly, a nanosecond (~5 ns pulse duration FWHM) Nd:YAG laser operated at its fundamental wavelength at 1064 nm with a repetition rate at 10 Hz was used. The maximum laser pulse energy of the laser was approximately 100 mJ/pulse. Instead of using a single plano-convex lens as previously reported [8], the laser beam was focused by a lens pair consisting of a plano-convex lens and a positive meniscus lens, each of a focal length of 10 cm. To minimize the laser fluence falling onto the window of the UF_6-containing chamber, the focusing-lens pair was placed flush with the chamber window. The laser induced plasma was formed roughly in the center of the chamber (cf. Figure 1).

A novel UF_6 corrosion-resistant sampling chamber was designed, fabricated and tested at Oak Ridge National Laboratory for use in this work. The internal volume of the chamber is about 270 cm^3. At room temperature, it takes 0.39 g of gaseous UF_6 to fill the chamber to its saturated vapor pressure of 80 torr. Two UF_6 sampling chambers were prepared and filled with UF_6 at different ^{235}U enrichment levels. One UF_6 sample is of natural uranium (NU) with ^{235}U abundance at 0.72 atom-% whereas the other is of low enriched uranium (LEU) with ^{235}U at

4.67 atom-%. The enrichment levels of the UF_6 samples were validated using a multi-collector inductively coupled plasma mass spectrometry (MC-ICP-MS). The respective chambers were loaded with 0.95 g of UF_6 for the NU sample and 0.70 g of UF_6 for the LEU sample. An excess UF_6, was added to the cell to allow for some consumption of the gas before the cell would need recharging, the excess material appears as white crystalline solid deposited at the bottom of the chamber.

Because its vapor pressure strongly depends on temperature [14], UF_6 pressure is varied indirectly but efficiently through temperature control at the bottom surface of the chamber. The chamber sits on a solid-state thermoelectric cooler (cf. Figure 1), which allows user-controllable setting of the UF_6 vapor pressure between ~ 80 torr (room temperature) and 5.5 torr (equivalent to a temperature of -13°C) within 10 minutes. The chambers contain UF_6 only, without any buffer gas, and each one is equipped with a pressure transducer (diaphragm type with a pizeo sensor, model 902B, MKS Instruments, Longmont, CO, USA). The LIBS spectra obtained in gaseous UF_6 (NU) samples were compared to those from a solid sample described in our previous study [8] prepared at the Y-12 National Security Complex. The uranium content was approximately 30% by weight [8] and contained ^{235}U at natural abundance level (i.e., 0.72 atom-%). LIBS measurement on this U-glass sample was performed under air at atmospheric pressure.

Plasma emission was collected with a fused-silica lens through another optical port of the sample chamber orthogonal to the laser, and directed to the entrance slit of the optical spectrometer through an optical fiber bundle (cf. Figure 1). The focal length of the spectrometer is 1.25 m (Horiba Jobin-Yvon 1250M, Longjumeau, France). Compared to our previous setup [8], the

ICCD detector was upgraded to a new one with a 25 mm ∅ intensifier and 2048 × 512 pixels (DH340T-25F-03, Andor, Belfast, Northern Ireland). The entrance slit of the spectrometer was set at 30 μm. With the exception of one study, as noted below, a grating with 3600 grooves/mm was used. The spectrometer was set to approximately 424.4 nm, and the measured spectral bandpass (instrumental broadening) was approximately 8 pm. For one particular measurement which required the simultaneous acquisition of the U II 424.437 nm and U II 430.146 nm lines, a grating with 2400 grooves/mm was used and the spectral bandpass was increased to about 16 pm. All presented data were corrected for dark counts of the ICCD detector. Furthermore, for measurements involving the two U II lines at 424.437 nm and 430.146 nm, the spectral response of the spectrometer–detector system was calibrated with a NIST traceable UV/VIS deuterium-halogen light source (AvaLight-DH-CAL, Avantes, Broomfield, CO, USA). For U isotopic analysis with spectral fitting, because the span of the spectral window was only 0.2 nm, spectral-response correction was not needed.

For measurements of the plasma temporal emission profiles, a series of 50 ICCD frames, each with progressively increasing detector gate delay and width, was acquired. The gate delay of a particular ICCD frame was set at the ending temporal window of the previous one, whereas the gate width was set to be 25 ns longer than the previous frame. This arrangement allows continuous monitoring of the temporal emission profile from 0 to almost 30 μs, with short enough gate width that each exposure can be regarded as a still frame showing the frozen plasma evolution. For the first frame, the delay and gate width were set at 0 and 25 ns, respectively (i.e., a temporal window from 0 to 25 ns) with respect to the onset of the laser. For the second frame, the delay and gate width were 25 and 50 ns, respectively (i.e., from 25 to 75 ns). For the third

and the fourth frame, the temporal windows were 75-150 ns and 150-250 ns, respectively. For the 10^{th}, 20^{th}, 30^{th} and 40^{th} frame, the temporal windows were 1.125-1.375 μs, 4.75-5.25 μs, 10.875-11.625 μs, and 19.5-20.5 μs respectively. The integrated exposure time for each ICCD frame was 8 s (i.e., accumulation of LIBS signal from 80 laser shots).

For U isotopic analysis and the measurements of the U II lines at 424.437 nm and 430.146 nm, the gate delay, gate width and integrated exposure time were all varied. Gate delay and width for each experiment will be noted in the pertaining discussions. For measurements with UF_6 at 15 and 6 torr, the integrated exposure time for each ICCD frame were 60 s (i.e., signal accumulation from 600 laser shots) and 120 s (i.e., 1200 laser shots), respectively.

3. Results and Discussion

3.1 Temporal evolution of U LIBS intensity with solid samples

As the present study is based on the previously developed LIBS method for solid samples [8], it is useful to use the emission characteristics of a solid sample as a reference. If the plasma emission behaviors are vastly different between the solid U-bearing and gaseous UF_6 samples, the likelihood that the method designed for solid samples can be *directly* applied for gaseous UF_6 becomes questionable. Particularly, because isotopic analysis is performed through multivariate nonlinear spectral fitting, a requisite for successful adaptation of the developed method [8] to gaseous UF_6 is comparable emission characteristics and spectral features between the two sample types. For instance, if additional spectral features are present in the UF_6 samples, the spectral-line fitting database needs to be modified to account for the additional lines. Therefore, an important strategy for the present work is to characterize and understand the difference of

laser induced plasma produced with solid sample and gaseous UF_6, and uncover the operating conditions that would result in comparable spectral characteristics as solid samples.

Figure 2 shows the temporally resolved LIBS spectra in the wavelength vicinity of 424 nm from the solid U_3O_8–$Li_2B_4O_7$ fused glassy sample [8]. The laser pulse energy was 100 mJ and was identical to that in our previous study [8]. Stark broadening and shift are functions of electron density and temperature of the plasma, and therefore, change with laser power and time as the plasma decays. As will be discussed later, the magnitudes of Stark broadening and shift follow exponential decay, and the decay constants for Stark width are larger than those of Stark shift. The delay times presented in Figure 2 were chosen in multiple (one to five) units of the decay constant (denoted by τ) of the measured U II 424.437 nm line width. For optical isotopic analysis with atomic lines, the detector delay time for spectral acquisition should be determined by the decay constant of the Stark effect. Both Stark broadening and shift are important and detrimental on isotopic analysis [8]. Line broadening blurs the separation of the isotopic peaks because isotopic shifts, even for large ones, are minute and are of similar magnitude as Stark broadening. Stark shift causes asymmetrical, often indeterminate, temporally integrated line profiles [8]. Accordingly, it is necessary to mandate a detector delay time sufficiently long so that almost all the Stark effect subsides. For an exponential decay, approximately only 5% and 2% of the effect remain, respectively, after three and four decay constants. Therefore, it is a good assumption that Stark effect largely subsides after three decay constants and can be considered as negligible after four decay constants.

The five time-resolved spectra depicted in Figure 2 are normalized to their individual baselines with an assigned value of 1. As such, signal-to-background ratio (SBR) can be readily inferred

from the displayed spectral peak height as these two parameters are related by SBR = height – 1. In this small wavelength region from 423.0 to 425.5 nm, the LIBS spectra for U are relatively simple. The strongest emission line in this spectral window is U II 424.166 nm followed by U II 424.437 nm (the one labeled with a vertical dotted line), which is the main spectral peak for U isotopic analysis with a pronounced isotopic splitting of -25 pm [8, 21, 22]. Because the U II 424.437 nm line contains the largest amount of information for isotopic analysis, it is used as the reference in subsequent discussion for SBR. Other relatively strong emission lines in this window are U I 423.167 nm, U II 423.204 nm, U I 423.604 nm, U II 424.059 nm, U I 424.626 nm, and U II 425.243 nm. Although many more U lines are present, they are significantly weaker compared to the reference U II 424.437 nm line and appear only as bumps in the baseline. As expected, peak width narrows and SBR improves as delay time increases from 1τ to 3τ (cf. Figure 2). The SBRs of the reference U II 424.437 nm peak were 2.3, 13, 20, 25 and 24 for delay times from 1τ to 5τ, respectively. The reasonably simple spectral features as presented in Figure 2 and the large SBRs for the U II 424.437 nm line for delay time $\geq 3\tau$ will be used as comparison benchmarks for LIBS spectra generated in gaseous UF_6.

3.2 Temporal evolution of U LIBS signal in gaseous UF_6 at room temperature

Figure 3a shows the time-resolved LIBS spectra from a gaseous UF_6 sample. No cooling was applied and the UF_6 vapor pressure was 80 torr; the chamber contains no buffer gas. Laser pulse energy was 100 mJ, identical to the case of the solid sample presented in Figure 2. The measured spectra from gaseous UF_6 are vastly different from those of the solid sample. First, many more spectral lines are registered in the UF_6 LIBS spectra. Many of these additional emission lines appear with similar intensity as the reference U II 424.437 nm line. These lines

belong to U (either neutral-atomic or ionic) and an expansion of the baseline from the solid-sample spectra (cf. Figure 2) reveals bumps at the same wavelength positions. These U lines are of high excitation potentials. The result that the laser induced plasma formed in gaseous UF_6 excites high-energy emission lines is regarded as undesirable as it complicates the spectra and requires substantial modification on the spectral-line database for fitting. Although the spectral features clean up a bit at longer delay times (e.g., at 4τ and 5τ), many U emissions are still strongly present. Second, SBRs are low; the SBR of the strongest line were only slightly larger than 1. For the reference U II 424.437 nm line, the SBRs were 1.3, 1.3, 0.95, 0.86 and 0.71 for delay times from 1τ to 5τ, respectively, i.e., decreasing with increasing delay time. Clearly, the characteristics of the laser induced plasma generated with a solid sample and gaseous UF_6 are different, and further characterization is needed to comprehend the effect of experimental conditions on the plasma behavior and the resultant spectra.

Figure 3b shows a similar set of time-resolved spectra but for decreased laser pulse energy of 15 mJ. Compared to the case with 100 mJ laser energy (cf. Figure 3a), two observations are noticeable. First, SBRs improved but were still low. The SBRs of the reference line for delay times from 1τ to 5τ were 3.0, 2.4, 1.8, 1.3 and 1.0, respectively. Second, those high-excitation potential U emission lines, which congest the spectra, show lower intensities compared to the main, lower-energy U lines (e.g., the eight prominent emission lines from the solid sample as discussed in Section 3.1). The effect is noticeable for the cluster of lines between 423.7 and 424.0 nm. With lower laser pulse energy, the plasma is weaker (which is also confirmed through visual inspection of the plasma brightness) but the complexity of the spectrum is reduced.

3.3 Effects of laser pulse energy and UF_6 pressure on temporally integrated spectra

The preceding discussion suggests that a weaker plasma is beneficial in simplifying the LIBS emission spectra from gaseous UF_6 sample. One objective of the present study is to locate the range of experimental conditions, specifically the laser pulse energy and the UF_6 gas pressure, so that the spectral characteristics (i.e., both the set of dominant emission lines and SBR behavior) are similar between UF_6 and solid samples. A total of 54 experimental conditions (9 settings on laser pulse energy from 8 to 100 mJ × 6 settings on UF_6 pressure from 10 to 80 torr) were studied, though not all studied combinations (i.e., those conditions in which both the laser energy and UF_6 pressure are low) lead to successful generation of a laser induced plasma.

Figure 4 shows the temporally integrated LIBS emission spectra from the gaseous UF_6 sample (the top four panels) and the U-glassy solid sample (the bottom panel). Detector gate width was fixed at 8 μs. Gate delays were varied in absolute time scale but were all started at 4τ of the individually measured Stark-width delay constants under each condition. These UF_6 spectra are representative of the four quadrants of the laser energy–UF_6 pressure combinations. First, let us take a look at the LIBS spectrum from a solid sample as it will be used as a comparison benchmark for UF_6 sample. Like the temporally resolved spectra presented in Figure 2, the temporally integrated LIBS spectrum of the U-glassy solid sample is comparatively simple and is in agreement with another published U spectra measured with LIBS [23]. The SBR of the reference U II 424.437 nm line was 22.2.

At high pressure (80 torr) and high laser pulse energy (100 mJ, the top panel of Figure 4), the temporally integrated spectra is congested with U emission lines of high excitation potential,

similar to the temporally resolved spectra presented in Figure 3a. The SBR of the U reference line was only 0.67. The relative intensities of those high-energy U lines slightly weakened and the SBR mildly improved to 0.87 as the laser pulse energy was lowered to 15 mJ (the second panel from the top). When the UF_6 pressure was reduced, SBR improved. A comparison of the LIBS spectra obtained under 10 torr (the third panel from the top) and 80 torr (the top panel) both under 100 mJ laser pulse energy reveals that, although the complexity of the spectra were somewhat similar, the SBR of the U reference line significantly enhanced to 5.5. Under the condition that both the laser pulse energy and UF_6 pressure were low (e.g., 20 mJ and 10 torr, the fourth panel from the top), the SBR further improved to 8.0 and the emission from those high-energy U lines diminished. Although there is some dissimilarity, for example, differences in the relative intensities among the dominant lines and degraded SBR, the overall characteristics of the LIBS spectra for gaseous UF_6 measured under low laser energy and UF_6 pressure are comparable to the reference spectra from the solid U sample. Figure 4 clearly concludes that UF_6 pressure is a more important parameter than laser pulse energy for direct LIBS analysis in gaseous UF_6.

3.4 Temporal characterization of LIBS signal and background from gaseous UF_6

The low SBRs from gaseous UF_6 sample and in particular their overall decreasing trends with delay time call for a closer examination on the temporal evolution of signal and background emission. Although the physics and expansion dynamics of the laser plasma are very different for solid and gaseous samples and a direct comparison on a fundamental level is beyond the scope of this study, it is still useful to note the phenomenological difference in the signal and background evolution between the two samples. Figure 5a shows the temporal evolution of the U II 424.437 nm emission line and its background from the solid U-glassy sample. Laser pulse

energy was 100 mJ. The behavior is typical for LIBS analysis of solid samples under atmospheric pressure and has been observed for many other samples. In brief, the analyte signal rapidly rises and reaches its maximum within 1 to 2 μs after the laser pulse and then decays. Background continuum emission is intense at the onset of the plasma formation and rapidly decays. Both the signal and the background can be described by a sum made up of two exponential decay functions (i.e., with a fast and a slow decaying component). Because the fast-decay component for the background is much quicker than that of the signal, SBR improves with delay time (up to a reasonable extent).

Figure 5b shows the evolution of the U line and its background for LIBS measurement of gaseous UF_6 at 80 torr with laser pulse energy of 100 mJ. Although the temporal behavior of the two curves can still be described by a two-component exponential decay, the fast-decay components of the U signal and its background are similar whereas the slow-decay component is longer for the background than for the signal. As a result, the background decays at a slower pace than the signal and SBR degrades with delay time. Similar behavior was observed in many combinations of laser pulse energy and UF_6 pressure. Only when both the laser pulse energy and the UF_6 pressure are low, the U signal and background decay at comparable rates. However, no studied experimental condition gave a fast decay for background but a comparatively slow decay for signal – the type of behavior that favors SBR as presented in Figure 5a.

The distinct difference between signal and background evolution between solid U-glassy and gaseous UF_6 samples triggers one to ask whether the observed behavior on UF_6 is generic for gaseous sample analysis with LIBS. To answer this question, another gaseous sample, (methylcyclopentadienyl)manganese(I) tricarbonyl (MMT), was tested. This Mn-containing

compound is in liquid form at room temperature and is volatile, although not as much as UF_6. A few drops of MMT were placed in another gas-sampling chamber, which contains air with a total pressure maintained at 80 torr. Figure 5c depicts the evolution of the Mn signal and its background. Surprisingly, the behaviors of the analyte (Mn) signal and its background adhere to the general observation of LIBS with solid samples (cf. Figure 5a) – that is, a speedy decay for background but a comparatively slower decay for signal, resulting in a favorable condition for SBR. In fact, the background emission in this case was significantly decayed after 6 μs to a level such that the measured background level was largely limited by the detector noise.

A hypothesis that can explain the unique temporal signal and background behavior of gaseous UF_6 sample is the recombination of U and F atoms. The observation of U atomic emission line obviously requires the complete breakdown of the six U–F bonds in a UF_6 molecule. Because both U and F atoms are unstable and highly reactive, they tend to recombine with each other when the plasma expands and cools. A fraction of the recombined molecular radicals is likely in an excited state capable of emitting photons through radiative de-excitation. The recombination plausibly proceeds in a stepwise fashion but even the simplest diatomic radial—UF—has highly crowded electronic excited states [24, 25], which can give rise to overlapping molecular emission like a pseudo-continuum. Emission from polyatomic species generally appears as broad, continuum-like structure. The recombination not only can increase the plasma background emission, but also quenches the population of free U atoms (and hence the U atomic emission signal).

This U–F recombination hypothesis is supported by literature examples [26, 27] and longevity of our UF_6 samples subjected to LIBS measurements. Laser ablation as an atom source combined

with reaction free-jet expansion is a powerful and commonly used technique in the field of molecular spectroscopy for the generation of gas-phase molecules [28-31]. Specific to U, reactions of laser-ablated U atoms with gases like F_2, ClF, Cl_2, and HF have been reported [26, 27, 31]. Hunt *et al.* [26] characterized the reaction products between F_2 (in an Ar gas buffer) and laser ablated U atoms and reported the presence of all the six fluorides, *viz.* UF, UF_2, UF_3, UF_4, UF_5, and UF_6 in the deposited matrix which was kept at a temperature of 12 K [26]. With annealing the matrix to a temperature of 35 K, the UF_6 product was reported to grow at the expense of other UF_x species and became the dominant one [26]. Clearly, recombination of U and F atoms proceeding all the way back to UF_6 is feasible and we believe that the same reaction takes place in our case because of the longevity of the loaded UF_6 in the sampling chamber. If one assumes that all the UF_6 molecules contained inside the physical volume of the laser induced plasma (approximately 1 mm in radius and 4 mm in length) are dissociated, each laser pulse would consume about 18 μg of UF_6. For our chamber in which ~ 1 g of UF_6 was loaded, the sample would last only for 56,000 laser pulses (i.e., less than 2 hours of continuous operation) before complete exhaustion. In marked contrast, the UF_6 sample chamber has undergone LIBS measurement time for at least several hundreds of hours and both the LIBS signal and gas pressure are still normal. The excess solid UF_6 loaded has not yet been entirely consumed. Although some experiments were performed at pressures lower than 80 torr on which the consumption rate calculation discussed above is based, most experiments were performed at pressure above 8 torr. In other words, the pressure factor could extend the lifetime by at most only one order of magnitude and would not be able to explain the longevity of the loaded UF_6 sample by more than two orders of magnitude. Based on our observations on the signal and

background temporal characteristics, and the longevity of the UF_6 sample, we believe that a significant fraction of U and F atoms are recombined all the way back to UF_6.

Another route, complementing the U–F recombination mechanism presented above, for the formation of excited polyatomic species that subsequently give continuum-like emission is incomplete dissociation of the UF_6 molecules. Fragments of UF_x (x = 1 to 5) can be formed directly by the high-temperature laser-induced plasma or through photo-dissociation of UF_6 molecules. Although there is no questions that some UF_6 molecules in or near to the volume containing the laser-induced plasma are dissociated completely to U and F atoms, other UF_6 molecules probably undergo only partial decomposition to give UF_x (x = 1 to 5) fragments because the laser-induced plasma must have a thermal gradient at its periphery. At its boundary, efficiency of chemical-bond dissociation decreases as the temperature of the plasma is lower. Yet, the plasma is energetic enough to break some, but not all, of the bonds in a UF_6 molecule to give respective molecular fragments. In addition, photo-dissociation of UF_6 molecules by UV emission of the plasma continuum is another source of molecular fragments. Photolysis of UF_6 to UF_5 is well documented in the literature [32-34] and is an efficient process with UV [35]. The absorption cross section of UF_6 rapidly rises from the order of 10^{-22} cm^2 at ~420 nm to 10^{-17} cm^2 at ~200 nm [36].

3.5 Temporal characterization of Stark width and shift of U II 424.437 nm peak in LIBS spectra from gaseous UF_6 and solid U-glass sample

The understanding of the evolution of Stark width and shift is essential for optical isotopic analysis because the Stark effect contributes to distortion of the measured spectral-line shape and

the apparent separation of the isotopic peaks. The width and shift of the U II 424.437 nm emission line were investigated under different combinations of laser pulse energy and UF_6 pressure. For all conditions studied, the measured line width and shift are well described by exponential-decay functions. Figure 6a displays a representative case with 20 mJ laser pulse energy and 30 torr UF_6 pressure. The measured width of the U II 424.437 nm line was 0.0204 nm at a delay time of 0.8 μs and decay with a time constant of 0.987 μs to an asymptotic value of 0.0084 nm, which is limited by instrumental broadening. The pre-exponential factor, which defines the width at zero-time delay, was 0.027 nm. Likewise, at 0.8 μs, the measured shift was -0.0036 nm (i.e., a blue shift). The pre-exponential factor and the decay constant for the shift were -0.010 nm and 0.858 μs, respectively. The asymptotic value of 0.0004 nm for the shift is an artefact caused by imperfect wavelength calibration of the spectrometer.

Figure 6b shows the temporal response of the measured width and shift of the U II 424.437 nm line with the solid U-glass sample. Because the laser pulse energy was much higher (100 mJ) than in the case of the UF_6 sample presented in Figure 6a and laser–material coupling is more efficient for a solid than for a gaseous sample, the plasma is stronger. As a result, compared to Figure 6a, decay constants as well as the pre-exponential factors are larger for both the measured width and shift.

Figure 7a compares the measured decay constants of line width and shift of the U II 424.437 nm line under different combinations of laser pulse energy and UF_6 pressure. The error bars represent the uncertainties associated with the exponential fittings. Overall, the decay constants for line width and shift are different. The dotted line shows the hypothetical situation in which the decay constants of line width and shift would be identical. For most conditions, line width

decay is slower than line shift (cf. Figure 7a). However, for conditions in which both the laser pulse energy (e.g., ≤ 25 mJ) and UF_6 pressure (e.g., ≤ 20 torr) are low, line shifts take slightly longer to decay than the widths. The four measurements under the four highest pressures (80, 60, 42 and 30 torr) with the highest laser pulse energy (100 mJ) deviate the most from the dotted line in Figure 7. Substantial deviations are also present for measurements under the three highest studied pressures with the second highest laser power (60 mJ). As will be discussed in Section 3.7, severe self-absorption is present for the resonance U II 424.437 nm line in LIBS analysis with gaseous UF_6 sample. Optical thickness of the line causes significantly slower decays (larger decay constants) of the measured width compared to shift.

Figure 7b depicts the relationship between the pre-exponential factor of the measured line width and shift. This pre-exponential factor governs the magnitude of the corresponding width or shift at the onset of plasma, and a good correlation was found. In all cases, the pre-exponential factors of Stark shift are significantly smaller than that of Stark width. The linear regression line almost passed through the origin with a slope of -0.364.

3.6 Spectral window centered at 424.44 nm for UF_6 enrichment assay

Based on the preceding fundamental characterization of the signal, background, and the Stark width and shift, multivariate nonlinear spectral fitting was applied to the LIBS spectra acquired from gaseous UF_6 sample. Several laser pulse energies under two UF_6 pressures (15 and 6 torr) were tested. Figure 8a shows representative spectra collected from the NU (with 0.72% ^{235}U) and LEU (with 4.67% ^{235}U) UF_6 samples. The isotopic splitting between the ^{235}U–^{238}U line pair at 424.412–424.437 nm is unambiguously identifiable, confirming the practical feasibility to

perform enrichment assay directly on gaseous UF_6 samples in laser induced plasmas. Figure 8b summarizes the determined ^{235}U content under different conditions for the LEU sample. The detector delay time was optimized for each condition by taking into account the decay of the Stark effect. In all cases, large positive biases were observed in the determined ^{235}U abundance. For the measurements with 15 torr UF_6, the determined ^{235}U contents for the same LEU sample exhibited a monotonic increasing trend from 6.06% (15 mJ laser pulse energy) to 9.91% (60 mJ), whereas the reference value as determined by MC-ICP-MS is only 4.67%. The large error bars at lower laser pulse energies (e.g., 15 and 20 mJ) were caused by the comparatively weak emission signals under those conditions. For measurements under 6 torr of UF_6, the determined ^{235}U contents ranged from 5.77% to 7.15%. The systematic biases were lessened yet still significant.

To investigate the source of this large systematic bias, the fitted spectra and the fitting residuals were examined. Figure 8c presents the measured, the fitted, the decomposed ^{235}U and ^{238}U components, and the fitting residual of the spectrum collected under 15 torr UF_6 and 40 mJ laser pulse energy. This particular example is selected as the determined ^{235}U content was 9.37% (cf. Figure 8b), which is double the 4.67% reference value. If the positive bias is caused by a misfit, it should become apparent through a visual inspection of the fitted spectrum. Overall, the experimental spectra were well fitted, and similar fitting qualities also were observed for spectra taken at other conditions. Specifically, the isotopic peak from ^{235}U at 424.412 nm was well fitted. The span of fitting residual ($\Delta \approx 2740$) in Figure 8c is about 7.5% of the span of the experimental spectra ($\Delta \approx 33100$), which is only slightly larger than those in our previous work with LIBS of solid samples [8], which ranged from 4.9% to 6.3%.

3.7 Problem of self-absorption and its verification

The good overall fitting quality but large deviated results for the determined ^{235}U content as presented in Figure 8b suggests that the systematic bias is unlikely caused by an artefact in the fitting algorithm and points to a source of a more fundamental nature. A visual examination of the measured spectra normalized to the U II 424.437 nm (i.e., the ^{238}U component) spectral peak and its baseline with assigned values of 1 and 0, respectively, revealed that the normalized ^{235}U profiles exhibited notable increments with rising laser pulse energy. Through independent experimental means, we confirmed that the analytical bias shown in Figure 8b is a result of self-absorption.

Self-absorption is a common problem reported for quantitative analysis with LIBS [37-40] and could cause the phenomenon observed in Figure 8b. To elaborate, among other factors, self-absorption is proportional to the number densities of the absorbing species (the ^{235}U and ^{238}U isotopic atoms in this case). When the emitted photons travel from the center portion of the plasma to the periphery, part of the emission could be reabsorbed because some atoms (here, the term "atoms" collectively refer to neutral atoms or atomic ions) belonging to the same species but in an electronic state capable of absorbing the emitted radiation are almost always present. The total absorption depends on the number density, absorption cross section, and the absorption path length. For a UF_6 sample with 4.67% enrichment, number density of ^{238}U atoms is roughly 20× that of ^{235}U. As a result, if self-absorption occurs, there is much more self-absorption for ^{238}U than for ^{235}U. Although the emission from both the ^{235}U and ^{238}U atoms are being re-absorbed, because self-absorption is non-linear with respect to number density of the absorber, the ^{238}U emission is being absorbed to a greater extent. Consequently, the ^{235}U peak appears to

be larger than it should be compared to the more-attenuated ^{238}U counterpart and causes a positive bias in the determined ^{235}U content.

The self-absorption hypothesis was experimentally confirmed with the ratio of a pair of emission line which share a common lower energy state (in this specific case, it is the ground state, i.e., U II 424.437 nm is a resonance line). Ideally, different components from a multiplet should be used [41, 42], but because a nearby multiplet for the U II 424.437 nm line could not be found, a line with comparable excitation energy (the U II 430.146 nm) was used instead. Because the excitation energy of both the U II 424.437 nm and the U II 430.146 nm lines are very close (cf. Figure 9a, $\Delta E = 0.0387$ eV), the intensity ratio of this line-pair should be insensitive to temperature and very close to a constant in the *absence* of self-absorption. In contrast, if the emission line intensity ratios show deviations with experimental conditions, it can be regarded as conclusive evidence of self-absorption. The duplicating mirror method [43]—another commonly used method for checking self-absorption of plasma—cannot be readily applied to our setup because the UF_6 chamber has only three optical windows. The laser beam needs to enter and exit the chamber through two windows to avoid ablation of any chamber wall material.

Figure 9b displays representative spectra of this U II line pair. A grating with lower groove density had to be used so that both U II lines could be measured simultaneously. The spectral resolution was degraded but was still adequate. Furthermore, several spectral atlases [23, 44, 45] were consulted to confirm the spectral purity (i.e., no direct-overlapping emission line) of the U II 430.146 nm line. In fact, there are two other U II resonance lines at 420.435 nm and 428.786 nm, which are even closer to the U II 424.437 nm line; however, they suffer spectral

interference from other U lines and therefore are not used. Emission signals for the two desired U II peaks were decomposed and evaluated through spectral fitting (cf. Figure 9b).

The measured intensity ratios of the U II 424.437 nm / U II 430.146 nm line pair at an UF_6 pressure of 15 torr is presented in Figure 9c. The data unambiguously confirm that the U II 424.437 nm line suffered from self-absorption for three reasons. Through published values of the oscillator strengths (*f* values) of these two U II lines, theoretical ratios at various assumed temperatures can be calculated. Table 1 shows the *gf* factor [45-47] of this pair of U II lines. As emission intensity, I_{21}, of an atomic line transitioning between state 2 and 1 is proportional to:

$$I_{21} \propto N_2 \frac{g_1}{g_2} \frac{1}{(\lambda_{21})^3} f_{12} \tag{1}$$

where N_2 is the number density of atoms at excited level 2, g_1 and g_2 are the degeneracy of the lower and upper levels 1 and 2, respectively, λ_{21} is the transition wavelength, and f_{12} is the oscillator strength of the transition. In this case, because the U II 424.437 nm and U II 430.146 nm line pair share the same lower state and the degeneracies of their upper states are coincidently identical, the intensity ratio of this line pair is further simplified to:

$$\frac{I_{U\ II\ 424.437}}{I_{U\ II\ 430.146}} = \left(\frac{430.146}{424.437}\right)^3 \frac{f_{U\ II\ 424.437}}{f_{U\ II\ 430.146}} exp\left(\frac{-E_{U\ II\ 424.437} + E_{U\ II\ 430.146}}{kT_{exc}}\right) \tag{2}$$

where $E_{U\ II\ 424.437}$ and $E_{U\ II\ 430.146}$ are, respectively, the excitation potential of the U II 424.437 nm and U II 430.146 nm lines, *k* is the Boltzmann constant and T_{exc} is the excitation temperature.

Also plotted in Figure 9c are some theoretical line pair ratios at various hypothetical plasma excitation temperatures. It should be emphasize again that, for this experiment, the spectrometer and detector system were calibrated for its spectral response. In agreement with previous discussions, this ratio is rather insensitive to plasma excitation temperature. For instance, the theoretical ratio is 2.81 if the exponential term is neglected (i.e., assuming infinite temperature) and reduced to only 2.57 for a temperature of 5000 K. The measured ratios span between 1.68 and 1.98, which according to thermodynamic model, infer excitation temperatures below 1500 K. Although the excitation temperature of the laser induced plasma is unknown, a realistic lower bound is at least 3000 K.

Second, the self-absorption hypothesis still stands even if one ignores the theoretical-ratio argument presented above (perhaps because an authoritative compilation of critically evaluated oscillator strength or transition probability is not yet available for uranium, or there is doubt on the uncertainty associated with the spectral-response calibration) but just compares the relative U II 424.437 nm / U II 430.146 nm ratio (R) under different experiment conditions. According to Boltzmann distribution, a change in the ratio (ΔR) is related to a change in temperature (ΔT) through:

$$\frac{\Delta R}{R} = \frac{\Delta E}{kT^2}\Delta T = \frac{449}{T}\left(\frac{\Delta T}{T}\right) \quad (3)$$

where ΔE is the energy difference of the two U lines (0.0387 eV) which translates to 449 K (in kT unit). If there is no self-absorption, a decline of the ratio from 1.98 to 1.68 (–15.1%) is unrealistically large for the small difference in the excitation energies of these two lines. If one assumes an initial plasma temperature of several thousand Kelvin, this extent of decrease in the

line ratio corresponds to several thousand Kelvin drop in plasma temperature (cf. Equation 3). Clearly, such a dramatic change in the line ratio is thermodynamically unrealistic. In addition, one should expect either an increase or no significant change, but not a decrease, in plasma temperature for increased laser pulse energy. However, the experimental data exhibited a decrease in ratio with increase in laser energy.

Third, as the oscillator strength of the U II 424.437 nm line is larger than that of the U II 430.146 nm line [45-47], if the ground state causes self-absorption for both U lines, the stronger emitting U II 424.437 nm line would exhibit larger self-absorption [48]. Because it is reasonable to expect that for higher laser pulse energy, more energetic the plasma and thus more U free atoms and ions are created, a declining trend in the line ratio as a result of more severe self-absorption is expected and indeed experimentally observed with rising laser pulse energy. Likewise, the self-absorption of the U II 424.437 nm line also caused positive bias as outlined above in the determined ^{235}U content (cf. Figure 8b).

3.8 Attempts to minimize and compensate for self-absorption

The effect of plasma operating parameters (namely: detector delay time, UF_6 pressure, and laser pulse energy) on self-absorption in gaseous UF_6 sample was studied. The objective was to understand and locate operating conditions that self-absorption was hopefully absent. In this experiment, the spectra were acquired in a temporally resolved fashion with 1 μs detector gate width whereas the detection gate delay was scanned from 2 μs to 7 μs, in steps of 1 μs, after the laser pulse. A total of thirty combinations with five UF_6 pressures (from 10 to 30 torr) and six laser pulse energies (from 10 to 60 mJ) were studied. Figure 10 presents the determined ^{235}U

contents of the LEU UF_6 sample as a function of detector delay time for some representative UF_6 pressures and laser energies.

Although the delay time has an effect in reducing the extent of self-absorption in some cases and makes the determined ^{235}U contents closer to the reference value of 4.67%, the deviations are still considerable. Further increasing the delay time to beyond 7 μs is not practical because the signal levels become too weak for reliable measurements in many cases with low UF_6 pressure and low laser pulse energy. In addition, because there is still a substantial difference between the determined ^{235}U and the reference values, it is unlikely that self-absorption can be reduced to a negligible level by simply lengthening the delay time. In contrast, the reduction of self-absorption (gauged from the difference between the determined ^{235}U and the reference values) was significant when either the laser pulse energy (cf. 10 torr UF_6, 60 mJ *vs.* 40 mJ) or the UF_6 pressure (40 mJ, 12 torr *vs.* 10 torr UF_6) were reduced. Clearly, optimization of laser pulse energy and UF_6 pressure is a more effective means to reduce self-absorption than the detector time delay. However, as already presented in Figure 8b, even reducing the UF_6 pressure to 6 torr – a level close to the breakdown threshold with 15 mJ laser pulse energy, self-absorption still persists. Further lowering the UF_6 pressure through cooling of the chamber is of limited practicality because of the temperature required as well as the proportionally reduced number density of UF_6 molecules available for measurement.

Another attempt to compensate for self-absorption was through implementation of a correction term in the fitting algorithm. This is in principle feasible because self-absorption causes distortion and broadening in the spectral peak shape [42], which provides a basis for its compensation. Several algorithms had been built and tested. Although some satisfactory results

were obtained under some conditions, more testing showed that the validity domain of all these examined algorithms were rather narrow and not robust to be applicable under wide-enough operation conditions that likely would be encountered in the field. Here, we define satisfactory performance as matching the ^{235}U reference value of the LEU UF_6 sample within at most a few percent in the relative scale, and ideally within a fraction of a percent. This high level of accuracy and precision is demanding but is what normally would be required for nuclear safeguards application. Because none of these evaluated algorithms performed at a level that fits the purpose, only a brief account is given.

The assessed models for compensation of self-absorption were a simple two-component, heterogeneous-plasma model in which the emission and the (self) absorption regions are completely separated in space, and a homogeneous plasma model in which the plasma is regarded as one uniformly homogeneous body with simultaneous emission and absorption happening in the same space. For these two models, several absorption spectral-line profiles (i.e., Lorentzian, Gaussian and Pseudo-Voigt) were examined, with or without deconvolution of the instrumental profile of the spectrometer–detector system. A two-component homogeneous plasma model was also evaluated, but overfitting likely occurred. Furthermore, the self-absorption coefficient (SA) method [38, 39], which is based on changes in line width was also tested. Despite their different assumptions on the distribution of the absorbing species in the plasma, all these models gauge the extent of and correct for self-absorption (typically denoted by the parameter τ_{SA}) of the spectral peak based on the slight peak distortion and minute broadened width as in our cases.

We found that the result for the determined ^{235}U isotopic abundance is very sensitive to the fitting parameter τ_{SA}, which governs the self-absorption correction. We also noted that the fitting uncertainty of τ_{SA} was large and because τ_{SA} can be determined only with coarse precision, the precision of the determined ^{235}U content in the sample was also degraded. The large fitting uncertainty of τ_{SA} can be understood from the fact that this parameter is determined through the slightly distorted line profile and the minute difference in the spectral line width in the presence and absence of small self-absorption. Because there are only a very limited number (~ 10) of data points in the measured U II 424.437 nm spectral profile (cf. Figure 8c), and the instrumental broadening which is about 8 pm already transforms to 4 pixels, the available information is insufficient for robust fitting.

4. Conclusion

In this study, we characterized the U signal, background emission, Stark width and shift in the laser induced plasma formed directly in gaseous UF_6 samples. It was found that UF_6 vapor pressure is a crucial parameter for LIBS analysis. At 80 torr of UF_6 (i.e., room temperature without cooling), many U lines with high-excitation potential emit strongly and result in a crowded spectrum. In addition, background is elevated and signal-to-background ratio is low. Only with conditions in which both UF_6 vapor pressure and laser pulse energy are low, for example, less than 20 torr pressure and 30 mJ pulse energy, the overall LIBS spectral characteristics (e.g., dominant emission lines and SBR) for solid U sample and gaseous UF_6 become comparable. Although conditions with reduced UF_6 pressure and laser energy give less congested spectra with higher SBR, the absolute emission intensity becomes low and so a compromise is needed.

The temporal evolution of the LIBS signal and its background was investigated in detail. Only when both the UF_6 pressure and the laser pulse energy were low, did the U signal and background decay at comparable rates. In other experimental conditions, the background decayed at a slower pace and persisted for a considerably longer time than the signal; consequently, SBR degraded with delay time. The comparatively long-persisting plasma background but rapid-decaying signal is a special feature for UF_6 and is not generic for gaseous sample analysis with LIBS, as confirmed by another Mn-containing volatile compound. A hypothesis involving recombination of U and F atoms all the way back to UF_6 molecule is proposed, which quenches the U atomic species and boosts pseudo-continuum background through molecular emission from excited UF_x radicals. This recombination hypothesis is also supported by the longevity of the UF_6 sample in the loaded chamber.

Direct isotopic analysis of gaseous UF_6 was evaluated with multivariate nonlinear spectral fitting on the LIBS spectra for extraction of isotopic information. The overall fitting quality is good but systematic bias on the determined ^{235}U content was observed. The origin of the analytical bias was traced back to significant self-absorption of the U II 424.437 nm resonance line. Compensation for self-absorption, through implementation of a correction term in the fitting algorithm, was attempted but in vain. This outcome is not surprising because all fitting algorithms for self-absorption correction are based on the minute distortion in the measured spectral profile (after self-absorption) and there is simply not enough information (number of data points) in the spectral peak profile that allows the extent of self-absorption be determined to a high degree of accuracy. Although the isotopic analysis results were not satisfactory, the knowledge gained in the present study on the interplays between operating conditions (e.g., detector delay time, UF_6 pressure, and laser pulse energy) and spectral characteristics (e.g.,

signal and background behavior, dominant spectral-line features, and self-absorption) would be useful to guide experimental design for future work on direct gaseous UF_6 enrichment assay with LIBS. Because the identified main barrier is self-absorption on the U II 424.437 nm resonance line, the best approach to correct for self-absorption is by avoiding it. In fact, we learned from this study that other U lines need to be used. A new spectral window that does not suffer from self-absorption but with appreciable ^{235}U–^{238}U isotopic shifts has been located, and further investigation is currently underway.

Acknowledgment

This work was supported by the National Nuclear Security Administration's Defense Nuclear Nonproliferation Office of Research and Development of the U.S. Department of Energy under contract numbers DE-AC02-05CH11231 at the Lawrence Berkeley National Laboratory and DE-AC05-00OR22725 at the Oak Ridge National Laboratory. Zhenli Zhu acknowledges support from the China Scholarship Council (CSC).

References

1. X. Hou, B.T. Jones, Field instrumentation in atomic spectroscopy, Microchem. J. 66 (2000) 115-145.
2. A. Gałuszka, Z.M. Migaszewski, J. Namieśnik, Moving your laboratories to the field – advantages and limitations of the use of field portable instruments in environmental sample analysis, Environ. Res. 140 (2015) 593-603.
3. R.A. Crocombe, Portable spectroscopy, Appl. Spectrosc. 72 (2018) 1701-1751.
4. F.J. Fortes, J.J. Laserna, The development of fieldable laser-induced breakdown spectrometer: No limits on the horizon, Spectrochim. Acta Part B 65 (2010) 975-990.

5. J. Rakovský, P. Čermák, O. Musset, P. Veis, A review of the development of portable laser induced breakdown spectroscopy and its applications, Spectrochim. Acta Part B 101 (2014) 269-287.
6. R.C. Chinni, D.A. Cremers, L.J. Radziemski, M. Bostian, C. Navarro-Northrup, Detection of uranium using laser-induced breakdown spectroscopy, Appl. Spectrosc. 63 (2009) 1238-1250.
7. C. Rinaldi, M. Pozzi, N. Boggio, J. Vorobioff, Isotopic analysis of uranium by laser induced breakdown spectroscopy, Spectrochim. Acta Part B 167 (2020) 105841.
8. J. Song, G.C.Y. Chan, X. Mao, J.D. Woodward, R.W. Smithwick, T.G. Schaaff, A.C. Stowe, C.D. Harris, R. Zheng, V. Zorba, R.E. Russo, Multivariate nonlinear spectral fitting for uranium isotopic analysis with laser-induced breakdown spectroscopy, Spectrochim. Acta Part B 150 (2018) 67-76.
9. K. Touchet, F. Chartier, J. Hermann, J.-B. Sirven, Laser-induced breakdown self-reversal isotopic spectrometry for isotopic analysis of lithium, Spectrochim. Acta Part B 168 (2020) 105868.
10. C.A. Akpovo, L. Helms, L.T.M. Profeta, L. Johnson, Multivariate determination of ^{10}B isotopic ratio by laser-induced breakdown spectroscopy using multiple BO molecular emissions, Spectrochim. Acta Part B 162 (2019) 105710.
11. S.H. Amiri, S.M.R. Darbani, H. Saghafifar, Detection of BO_2 isotopes using laser-induced breakdown spectroscopy, Spectrochim. Acta Part B 150 (2018) 86-91.
12. S.-U. Choi, S.-C. Han, J.-I. Yun, Hydrogen isotopic analysis using molecular emission from laser-induced plasma on liquid and frozen water, Spectrochim. Acta Part B 162 (2019) 105716.
13. S.S. Harilal, B.E. Brumfield, N.L. LaHaye, K.C. Hartig, M.C. Phillips, Optical spectroscopy of laser-produced plasmas for standoff isotopic analysis, Appl. Phys. Rev. 5 (2018) 021301.
14. S.S. Sazhin, A.P. Jeapes, Fluorination of uranium dioxide particles: A review of physical and chemical properties of the compounds involved, J. Nucl. Mater. 275 (1999) 231-245.
15. H. Groult, F. Lantelme, M. Salanne, C. Simon, C. Belhomme, B. Morel, F. Nicolas, Role of elemental fluorine in nuclear field, J. Fluorine Chem. 128 (2007) 285-295.
16. J. Wu, Y. Qiu, X. Li, H. Yu, Z. Zhang, A. Qiu, Progress of laser-induced breakdown spectroscopy in nuclear industry applications, J. Phys. D: Appl. Phys. 53 (2019) 023001.

17. M.B. Shattan, M. Gragston, Z. Zhang, J.D. Auxier, II, K.G. McIntosh, C.G. Parigger, Mapping of uranium in surrogate nuclear debris using laser-induced breakdown spectroscopy (LIBS), Appl. Spectrosc. 73 (2019) 591-600.
18. E. Rollin, O. Musset, D. Cardona, J.B. Sirven, Laser-induced breakdown spectroscopy of uranium in the vacuum ultraviolet range, Spectrochim. Acta Part B 166 (2020) 105796.
19. G. Gautam, C.G. Parigger, C.M. Helstern, K.A. Drake, Emission spectroscopy of expanding laser-induced gaseous hydrogen–nitrogen plasma, Appl. Opt. 56 (2017) 9277-9284.
20. C.G. Parigger, Measurements of gaseous hydrogen-nitrogen laser-plasma, Atoms 7 (2019) 61.
21. Z. Hainski, G. Rossi, Isotopic analysis of uranium by an optical spectral method – I. Determination of U235 in natural and depleted uranium with DC arc excitation and photographic recording, Energia Nucleare 12 (1965) 306-309.
22. T. Lee, O.P. Killeen, S.A. MacIntyre, The spectrographic determination of uranium 235. Part IV. Using a direct reading, littrow, grating spectrograph and a hollow cathode, Appl. Spectrosc. 15 (1961) 106-109.
23. K. Akaoka, M. Oba, M. Miyabe, H. Otobe, I. Wakaida, Measurement of uranium spectrum using laser induced breakdown spectroscopy – high resolution spectroscopy (350-470 nm), JAEA-Research 2015-012, Japan Atomic Energy Agency, (2015).
24. I.O. Antonov, M.C. Heaven, Spectroscopic and theoretical investigations of UF and UF^+, J. Phys. Chem. A 117 (2013) 9684-9694.
25. D.H. Bross, K.A. Peterson, Theoretical spectroscopy study of the low-lying electronic states of UX and UX^+, X = F and Cl, J. Chem. Phys. 143 (2015) 184313.
26. R.D. Hunt, C. Thompson, P. Hassanzadeh, L. Andrews, Matrix IR spectra of the products from fluorine molecule, chlorine molecule, and chlorine fluoride (ClF) reactions with pulsed-laser evaporated uranium atoms, Inorg. Chem. 33 (1994) 388-391.
27. T. Vent-Schmidt, L. Andrews, S. Riedel, Reactions of laser-ablated U atoms with HF: Infrared spectra and quantum chemical calculations of HUF, UH, and UF in noble gas solids, J. Chem. Phys. A 119 (2015) 2253-2261.
28. G.S. Grubbs, D.J. Frohman, S.E. Novick, S.A. Cooke, Measurement and analysis of the pure rotational spectra of tin monochloride, SnCl, using laser ablation equipped chirped pulse and cavity Fourier transform microwave spectroscopy, J. Mol. Spectrosc. 280 (2012) 85-90.

29. M.J. Dick, P.M. Sheridan, J.G. Wang, P.F. Bernath, A high-resolution laser ablation study of the A˜2Π–X˜2Σ$^+$ transition of SrCCH, J. Mol. Spectrosc. 233 (2005) 197-202.
30. A.A. Breier, B. Waßmuth, G.W. Fuchs, J. Gauss, T.F. Giesen, Mass-independent analysis of the stable isotopologues of gas-phase titanium monoxide – TiO, J. Mol. Spectrosc. 355 (2019) 46-58.
31. M.C. Heaven, B.J. Barker, I.O. Antonov, Spectroscopy and structure of the simplest actinide bonds, J. Chem. Phys. A 118 (2014) 10867-10881.
32. E. Borsella, F. Catoni, G. Freddi, Study of UF_6 photodissociation through light scattering of UF_5 particles, J. Chem. Phys. 73 (1980) 316-321.
33. P.M. Kroger, S.J. Riley, G.H. Kwei, Polyhalide photofragment spectra. II. Ultraviolet photodissociation dynamics of UF_6, J. Chem. Phys. 68 (1978) 4195-4201.
34. W.B. Lewis, F.B. Wampler, E.J. Huber, G.C. Fitzgibbon, Photolysis of uranium hexafluoride and some reaction variables affecting the apparent quantum yield, Journal of Photochemistry 11 (1979) 393-401.
35. V.Y. Baranov, Y.A. Kolesnikov, A.A. Kotov, Laser photolysis of UF_6 molecules, Quantum Electronics 29 (1999) 653-666.
36. G.L. DePoorter, C.K. Rofer-DePoorter, The absorption spectrum of UF_6 from 2000 to 4200 Å, Spectrosc. Lett. 8 (1975) 521-524.
37. D. Bulajic, M. Corsi, G. Cristoforetti, S. Legnaioli, V. Palleschi, A. Salvetti, E. Tognoni, A procedure for correcting self-absorption in calibration free-laser induced breakdown spectroscopy, Spectrochim. Acta Part B 57 (2002) 339-353.
38. A.M. El Sherbini, T.M. El Sherbini, H. Hegazy, G. Cristoforetti, S. Legnaioli, V. Palleschi, L. Pardini, A. Salvetti, E. Tognoni, Evaluation of self-absorption coefficients of aluminum emission lines in laser-induced breakdown spectroscopy measurements, Spectrochim. Acta Part B 60 (2005) 1573-1579.
39. F. Rezaei, G. Cristoforetti, E. Tognoni, S. Legnaioli, V. Palleschi, A. Safi, A review of the current analytical approaches for evaluating, compensating and exploiting self-absorption in laser induced breakdown spectroscopy, Spectrochim. Acta Part B 169 (2020) 105878.
40. J. Hou, L. Zhang, Y. Zhao, Z. Wang, Y. Zhang, W. Ma, L. Dong, W. Yin, L. Xiao, S. Jia, Mechanisms and efficient elimination approaches of self-absorption in LIBS, Plasma Sci. Technol. 21 (2019) 034016.

41. P.W.J.M. Boumans, Theory of spectrochemical excitation, Hilger & Watts Ltd., London, UK (1966).
42. N. Konjevic, M. Ivkovic, S. Jovicevic, Spectroscopic diagnostics of laser-induced plasmas, Spectrochim. Acta Part B 65 (2010) 593-602.
43. H.-Y. Moon, K.K. Herrera, N. Omenetto, B.W. Smith, J.D. Winefordner, On the usefulness of a duplicating mirror to evaluate self-absorption effects in laser induced breakdown spectroscopy, Spectrochim. Acta Part B 64 (2009) 702-713.
44. R. Payling, P. Larkins, Optical emission lines of the elements, John Wiley and Son, UK (2000).
45. B.A. Palmer, R.J. Engleman, R.A. Keller, An atlas of uranium emission intensities in a hollow-cathode discharge, LA-8251-MS, Los Alamos National Laboratory, (1980).
46. C.H. Corliss, Oscillator-strengths for lines of ionized uranium (U II), J. Res. Nat. Bur. Stand. Sec. A 80 (1976) 429-438.
47. A. Compant La Fontaine, Study of low-temperature uranium plasmas not within local thermodynamical equilibrium, J. Phys. B 20 (1987) 6649-6667.
48. R.C. Hilborn, Einstein coefficients, cross sections, *f* values, dipole moments, and all that, Am. J. Phys. 50 (1982) 982-986.

Table 1 *gf* values of the U II 424.437 nm and U II 430.146 nm emission lines [45-47].

Remark	U II 424.437 nm	U II 430.146 nm	$gf_{\text{U II 424.437}}$ / $gf_{\text{U II 430.146}}$
Corliss [46], relative *gf*	0.046	0.017	2.71
Compant La Fontaine [47] derived from Palmer *et al.* [45], relative *gf*	0.058	0.022	2.64
Compant La Fontaine [47], absolute *gf*	0.13	0.047	2.77
Average			2.71

Figure Captions

Figure 1 Photograph showing the experimental setup and generation of laser induced plasma directly in gaseous UF_6 at a pressure of 13.1 torr.

Figure 2 Temporally resolved LIBS spectra of a U-glassy solid sample measured at delay times of (from top to bottom panel) 0.90, 2.28, 3.00, 4.28 and 5.25 μs, which correspond to approximately one to five decay constants (τ = 1.06 μs) of the Stark width. Laser pulse energy was 100 mJ. Intensities are normalized to their respective individual baselines.

Figure 3 Temporally resolved LIBS spectra of gaseous UF_6 sample at 80 torr (i.e., room temperature) (a) The delay times (from top to bottom panel) were 1.95, 3.83, 5.78, 7.50 and 9.45 μs, which correspond to approximately one to five decay constants (τ = 1.89 μs) of the Stark width. Laser pulse energy was 100 mJ. (b) The delay times (from top to bottom panel) were 1.13, 2.63, 3.83, 5.25, and 6.33 μs, which correspond to approximately one to five decay constants (τ = 1.24 μs) of the Stark width. Laser pulse energy was 15 mJ. Intensities are normalized to their respective individual baselines.

Figure 4 Temporally integrated LIBS spectra of gaseous UF_6 and U-glassy samples. The sample and condition (from top to bottom panel) were (i) 80 torr UF_6, 100 mJ laser energy; (ii) 80 torr UF_6, 15 mJ laser energy; (iii) 10 torr UF_6, 100 mJ laser energy; (iv) 10 torr UF_6, 20 mJ laser energy; and (v) U-glassy solid sample, 100 mJ laser energy. Integration window started at four decay constants (i.e., 4τ) of the corresponding measured Stark width. Gate widths were 8 μs for all spectra. Intensities are normalized to their respective individual baselines.

Figure 5 Temporal evolutions of the U II 424.437 nm peak height and its background of (a) the U-glassy solid sample with 100 mJ laser energy; (b) 80 torr UF_6 with 100 mJ laser energy. (c) Temporal evolutions of the Mn II 259.373 nm peak height and its background of MMT in air at a total pressure of 80 torr with 100 mJ laser energy.

Figure 6 Temporal evolutions of the measured width and shift of the U II 424.437 nm line of (a) a UF_6 sample at 30 torr with 20 mJ laser pulse energy, and (b) a U-glass sample under air at atmospheric pressure with 100 mJ laser pulse energy. Both width and shift can be well represented by an exponential decay function.

Figure 7 Correlation of (a) exponential decay constants, and (b) pre-exponential wavelength factor between measured line shift and width of the U II 424.437 nm line.

Figure 8 (a) Experimentally measured LIBS emission spectra from two UF_6 samples (with 0.72% and 4.67% ^{235}U), showing the distinct isotopic peak from ^{235}U. Spectra were taken with UF_6 at a pressure of 6 torr and with laser pulse energy of 30 mJ. (b) Determined ^{235}U content of the LEU UF_6 sample (reference value of ^{235}U is 4.67%) with nonlinear spectral fitting with a database containing twelve line pairs. (c) Experimental LIBS and fitted spectra, and the fitting residual of the LEU UF_6 sample. Spectra were taken with UF_6 at a pressure of 15 torr and with laser pulse energy of 40 mJ. The wavelength positions of the ^{235}U and ^{238}U spectral peaks are marked by different symbols with vertical lines at the bottom of the figure.

Figure 9 (a) A schematic diagram showing the relative energy of the U II 424.437 nm and U II 430.146 nm emission lines, and the principle of how the emission ratio from this line pair can be used to gauge self-absorption. (b) Experimental LIBS and fitted

spectra of this U II line pair from a UF_6 sample (15 torr UF_6 and 30 mJ laser energy). (c) Measured and theoretical U II 424.437 nm / U II 430.146 nm ratios.

Figure 10 Determined ^{235}U content of the LEU UF_6 sample (reference value of ^{235}U is 4.67%) as a function of delay time. Gate width was fixed at 1 μs. Experimental conditions are as marked.

Figure

Figure 1

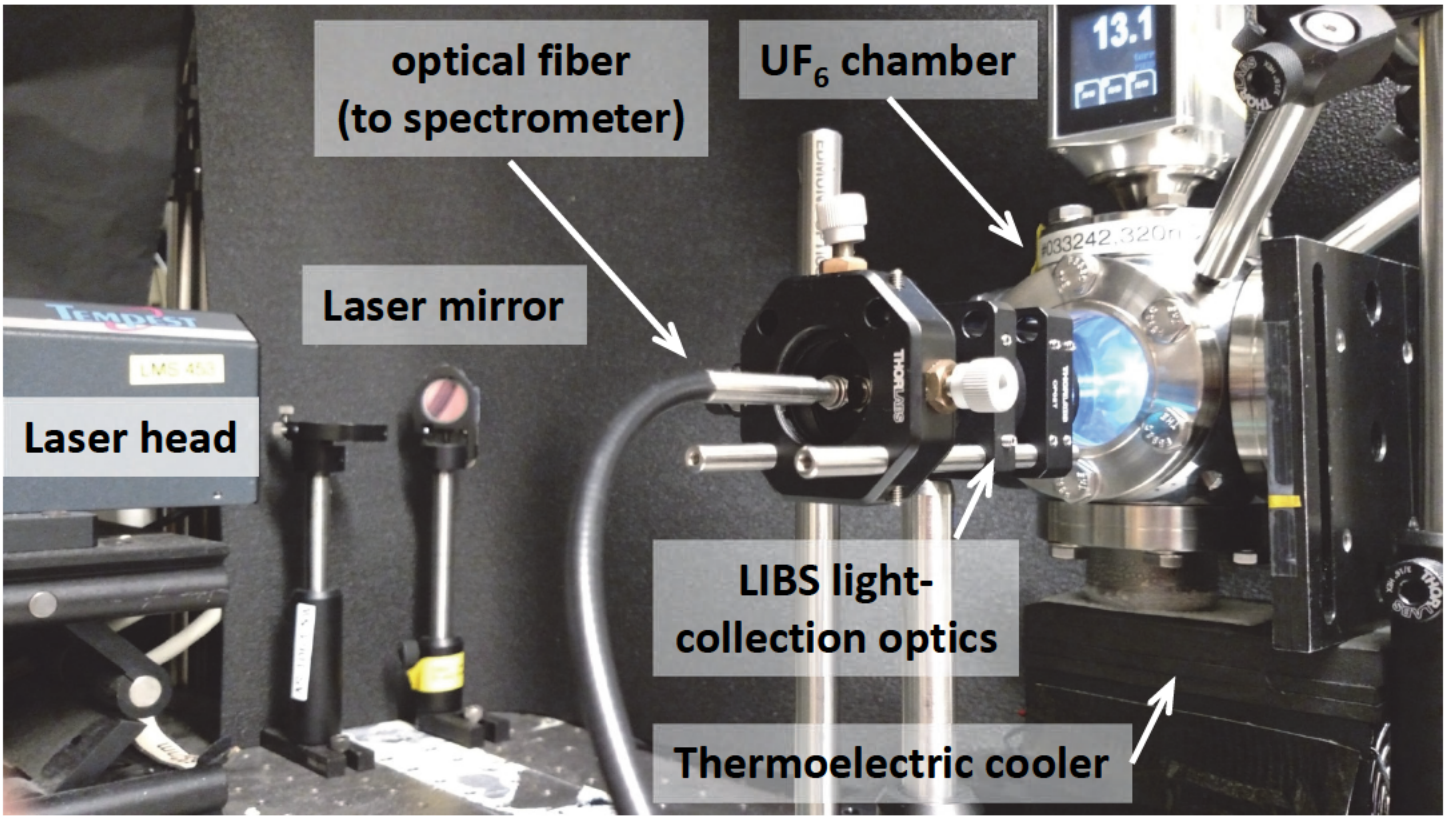

Figure 2

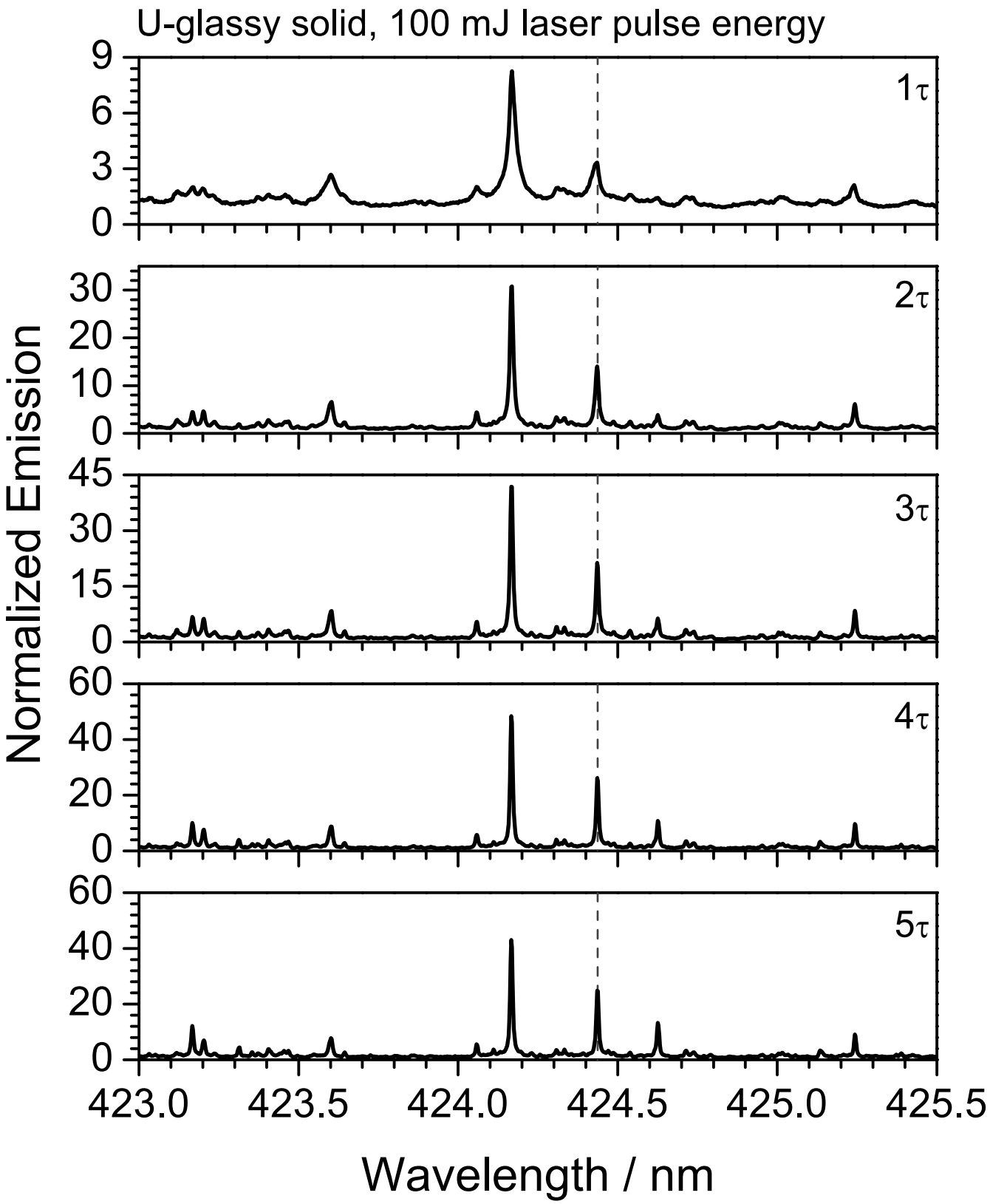
U-glassy solid, 100 mJ laser pulse energy
Normalized Emission
1τ
2τ
3τ
4τ
5τ
9
6
3
0
30
20
10
0
45
30
15
0
60
40
20
0
60
40
20
0
423.0
423.5
424.0
424.5
425.0
425.5
Wavelength / nm

Figure 3a

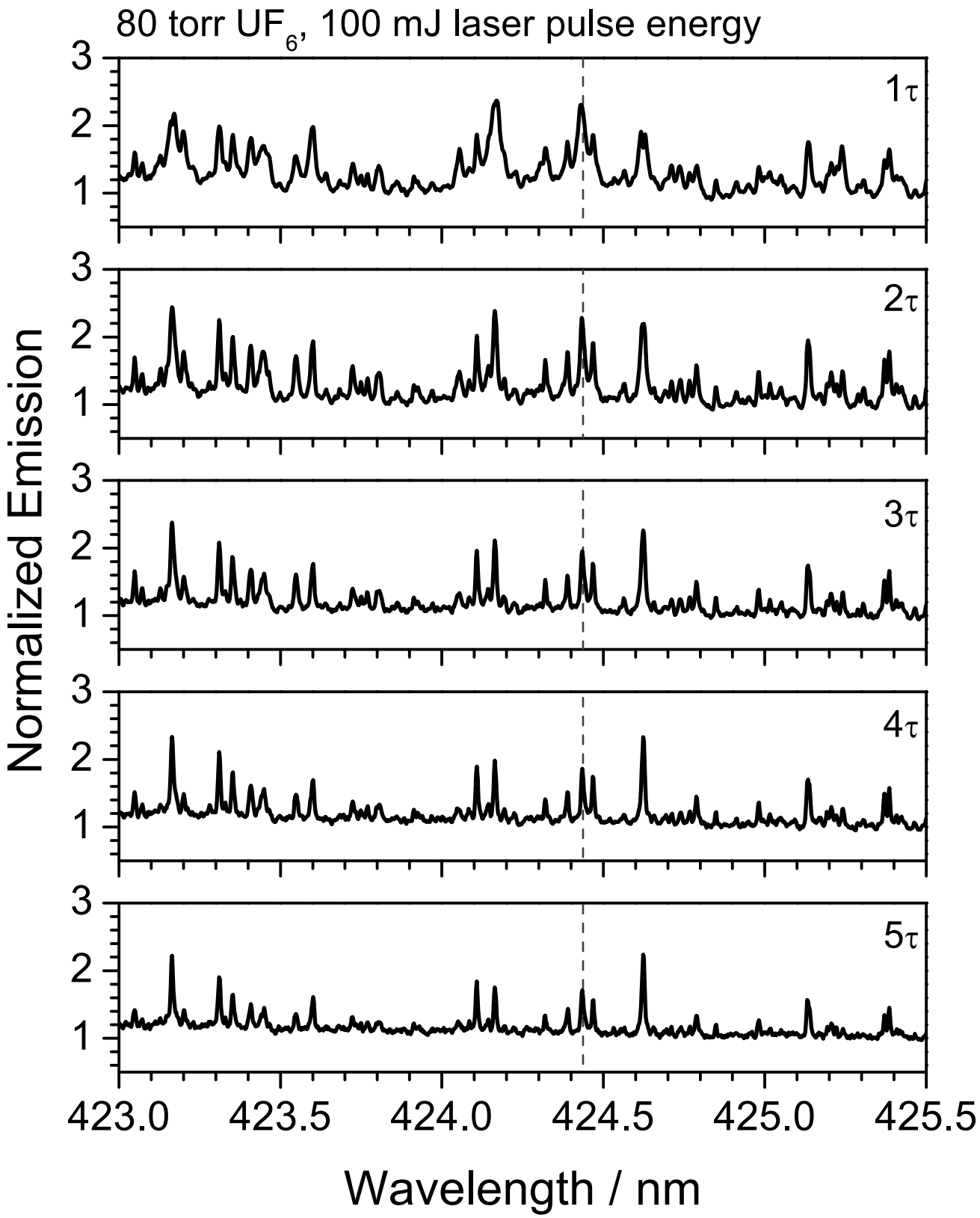
80 torr UF6, 100 mJ laser pulse energy
1τ
2τ
3τ
4τ
5τ
Normalized Emission
Wavelength / nm
423.0
423.5
424.0
424.5
425.0
425.5
1
2
3

Figure 3b

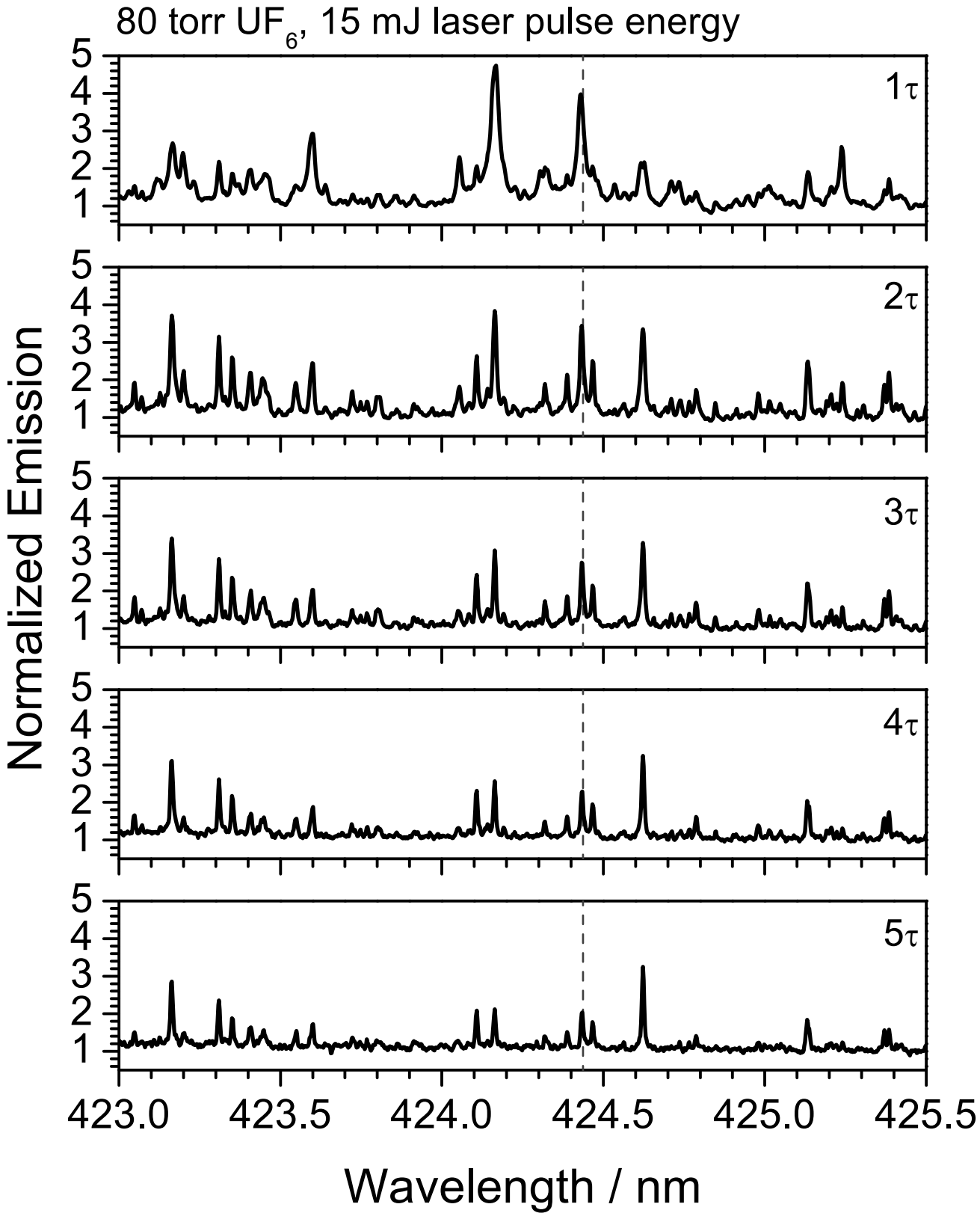
80 torr UF6, 15 mJ laser pulse energy
1τ
2τ
3τ
4τ
5τ
Normalized Emission
1
2
3
4
5
423.0
423.5
424.0
424.5
425.0
425.5
Wavelength / nm

Figure 4

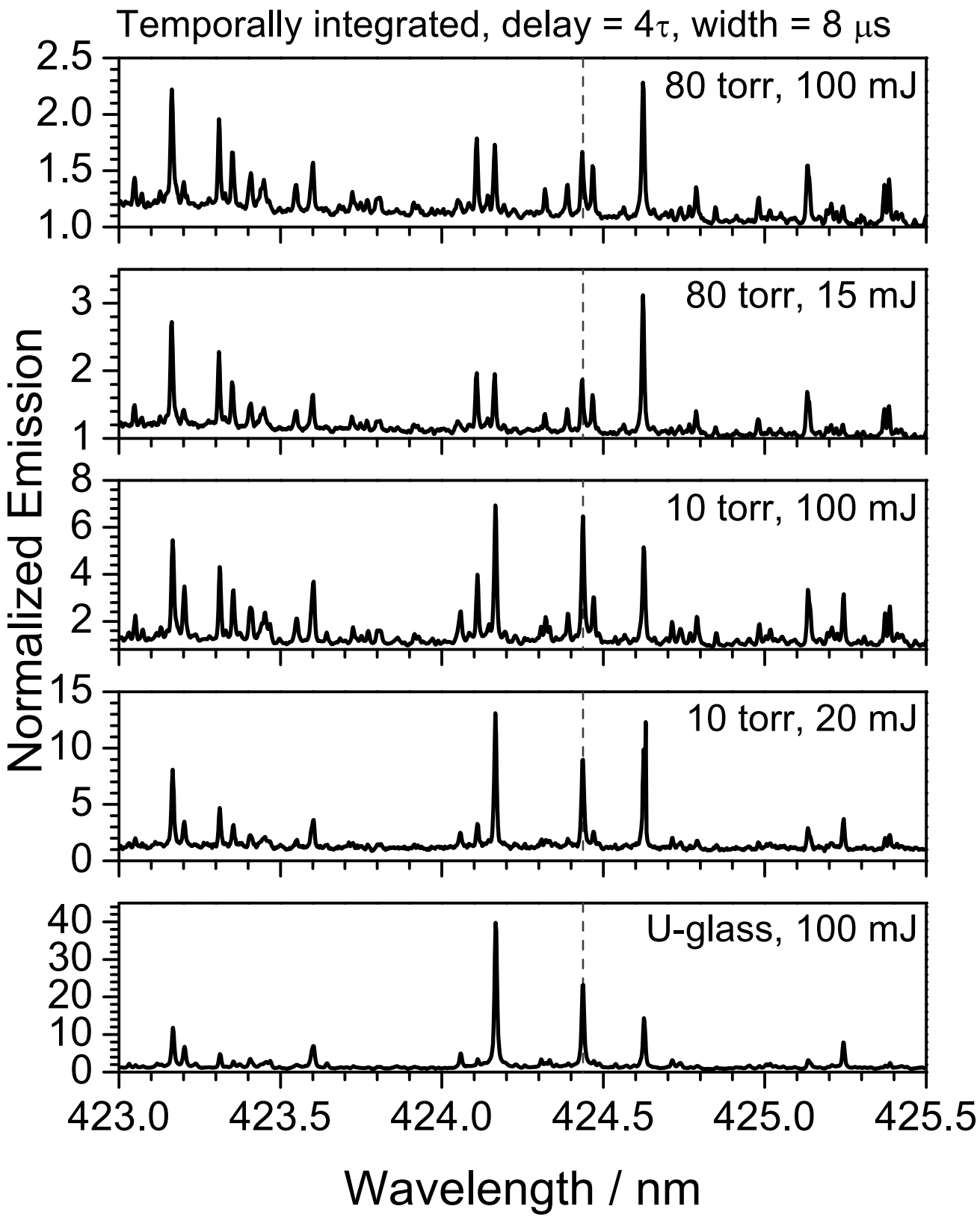
Temporally integrated, delay = 4τ, width = 8 μs
80 torr, 100 mJ
80 torr, 15 mJ
10 torr, 100 mJ
10 torr, 20 mJ
U-glass, 100 mJ
Normalized Emission
Wavelength / nm
423.0
423.5
424.0
424.5
425.0
425.5

Figure 5a

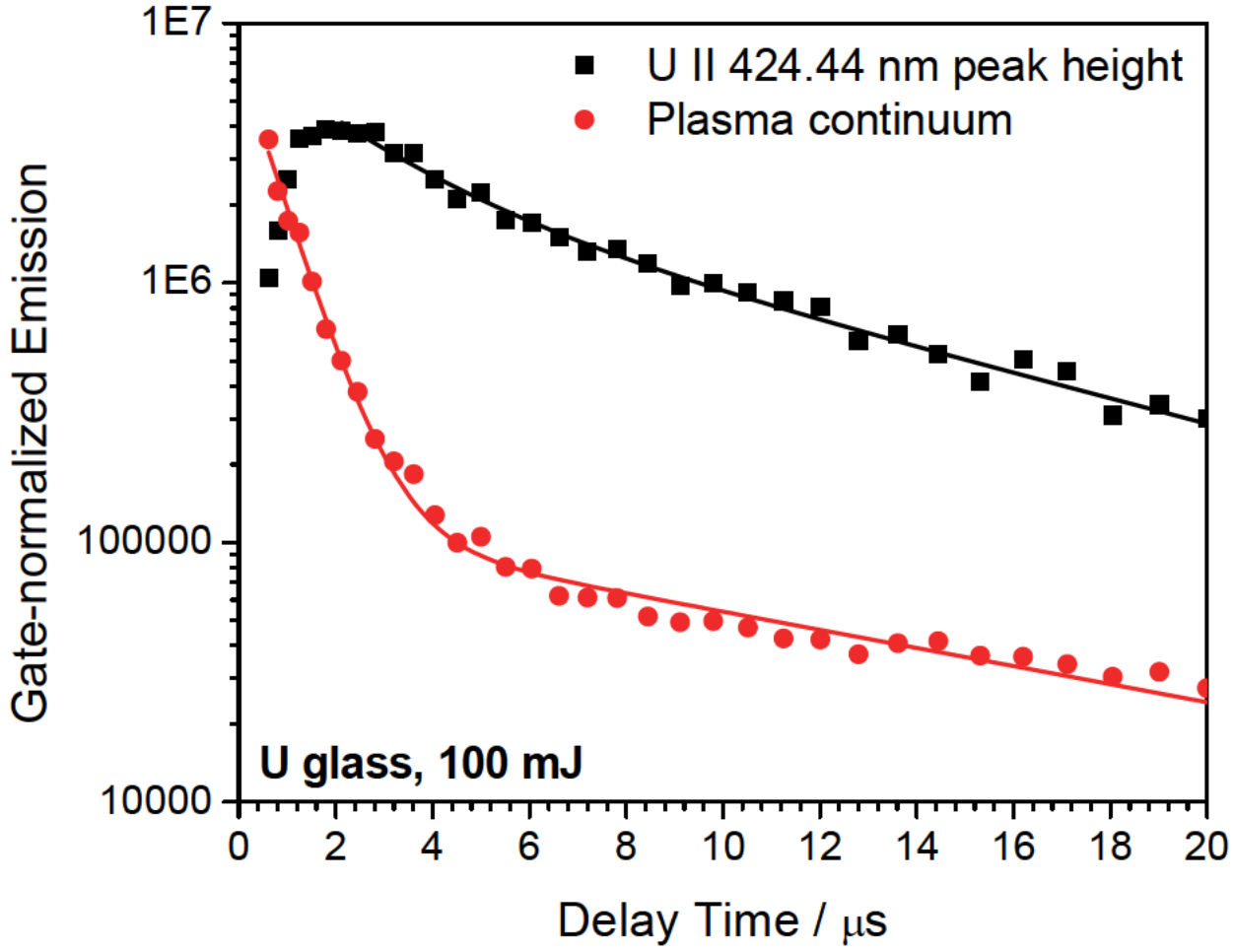
1E7
1E6
100000
10000
Gate-normalized Emission
U II 424.44 nm peak height
Plasma continuum
U glass, 100 mJ
0
2
4
6
8
10
12
14
16
18
20
Delay Time / μs

Figure 5b

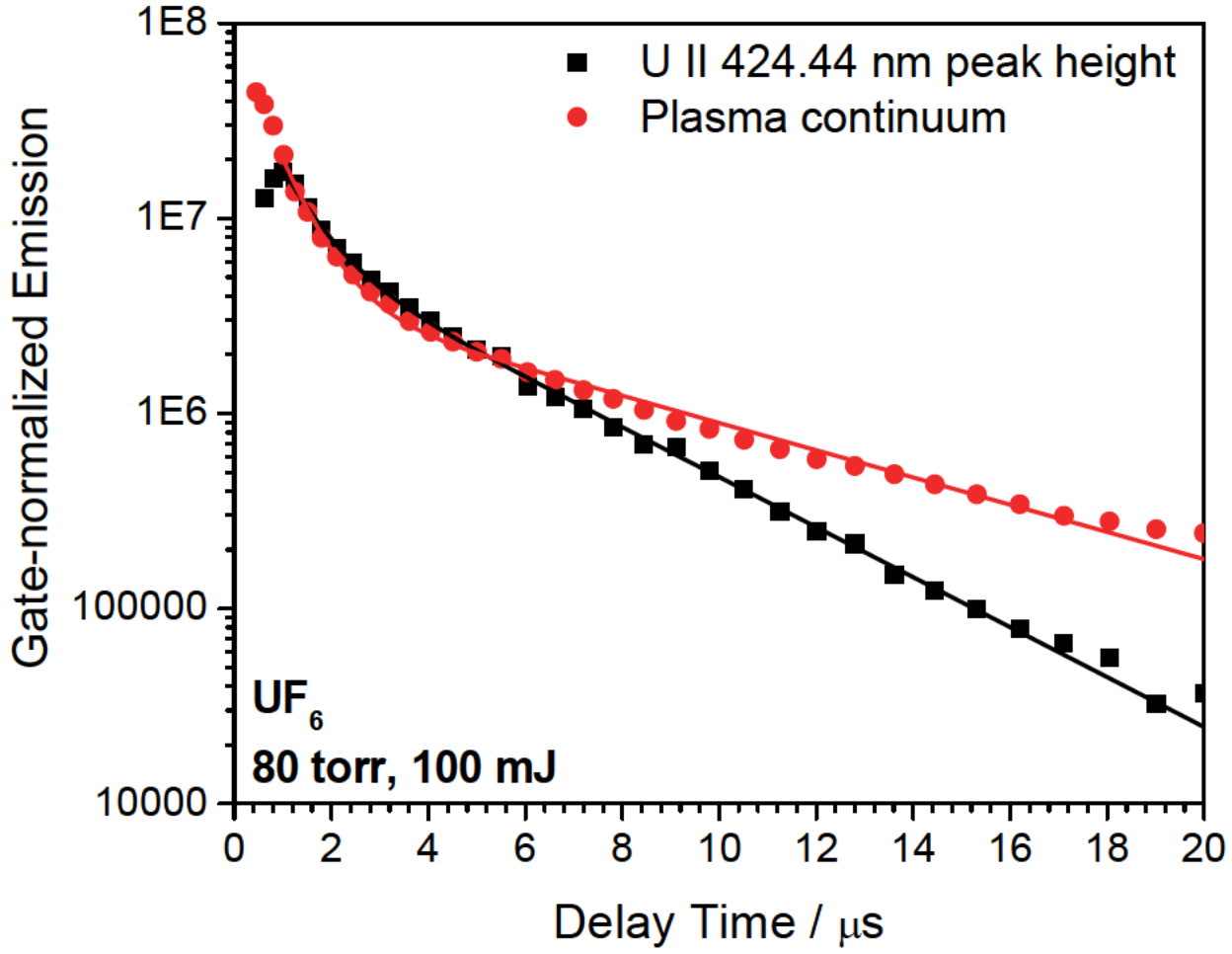
1E8
1E7
1E6
100000
10000
Gate-normalized Emission
U II 424.44 nm peak height
Plasma continuum
UF6
80 torr, 100 mJ
0
2
4
6
8
10
12
14
16
18
20
Delay Time / μs

Figure 5c

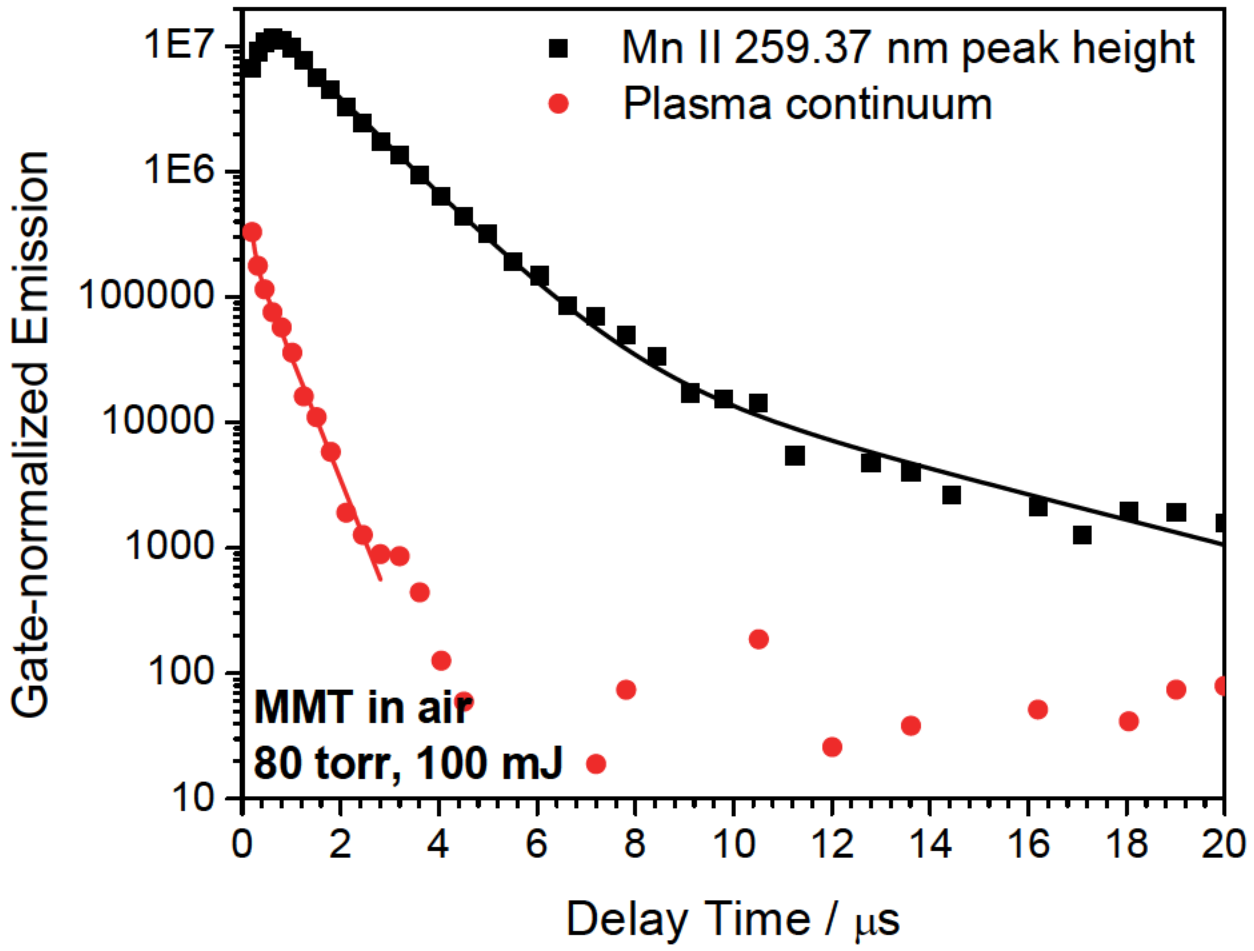
Mn II 259.37 nm peak height
Plasma continuum
MMT in air
80 torr, 100 mJ
Gate-normalized Emission
Delay Time / μs
1E7
1E6
100000
10000
1000
100
10
0
2
4
6
8
10
12
14
16
18
20

Figure 6a

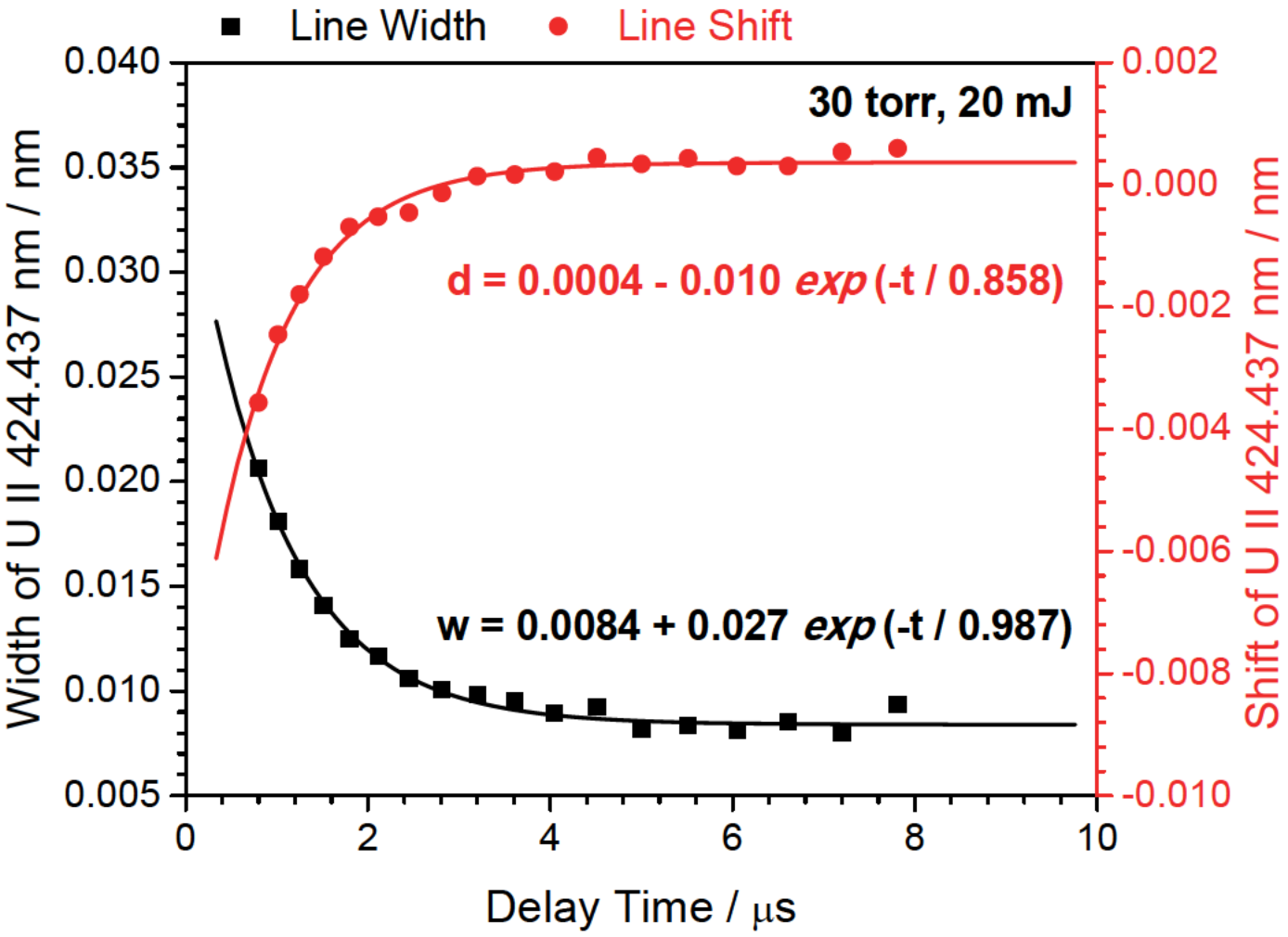
Line Width
Line Shift
30 torr, 20 mJ
d = 0.0004 - 0.010 exp (-t / 0.858)
w = 0.0084 + 0.027 exp (-t / 0.987)
Width of U II 424.437 nm / nm
Shift of U II 424.437 nm / nm
Delay Time / μs
0.040
0.035
0.030
0.025
0.020
0.015
0.010
0.005
0.002
0.000
-0.002
-0.004
-0.006
-0.008
-0.010
0
2
4
6
8
10

Figure 6b

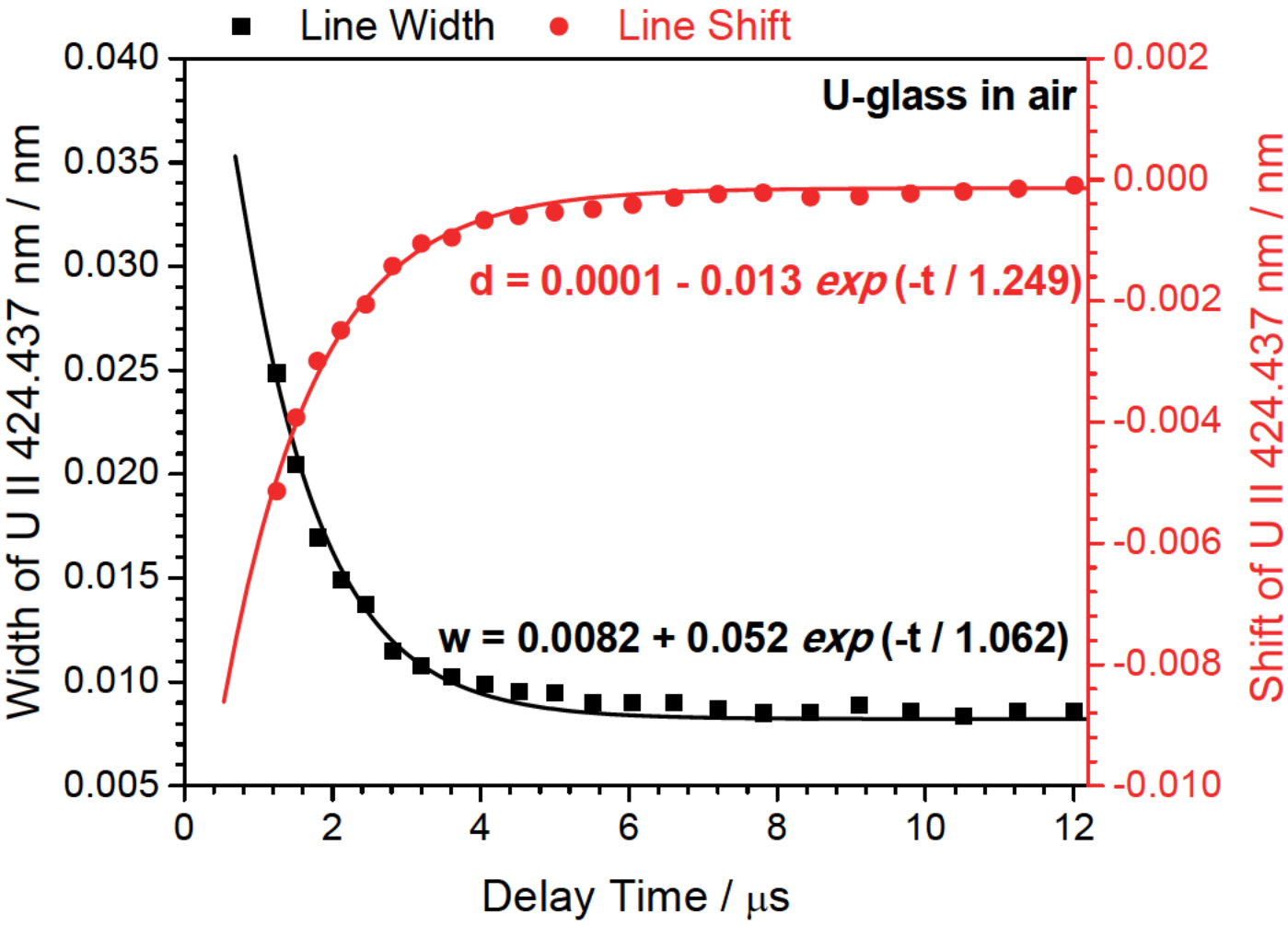
Line Width
Line Shift
U-glass in air
d = 0.0001 - 0.013 exp (-t / 1.249)
w = 0.0082 + 0.052 exp (-t / 1.062)
Width of U II 424.437 nm / nm
Shift of U II 424.437 nm / nm
Delay Time / μs
0.040
0.035
0.030
0.025
0.020
0.015
0.010
0.005
0.002
0.000
-0.002
-0.004
-0.006
-0.008
-0.010
0
2
4
6
8
10
12

Figure 7a

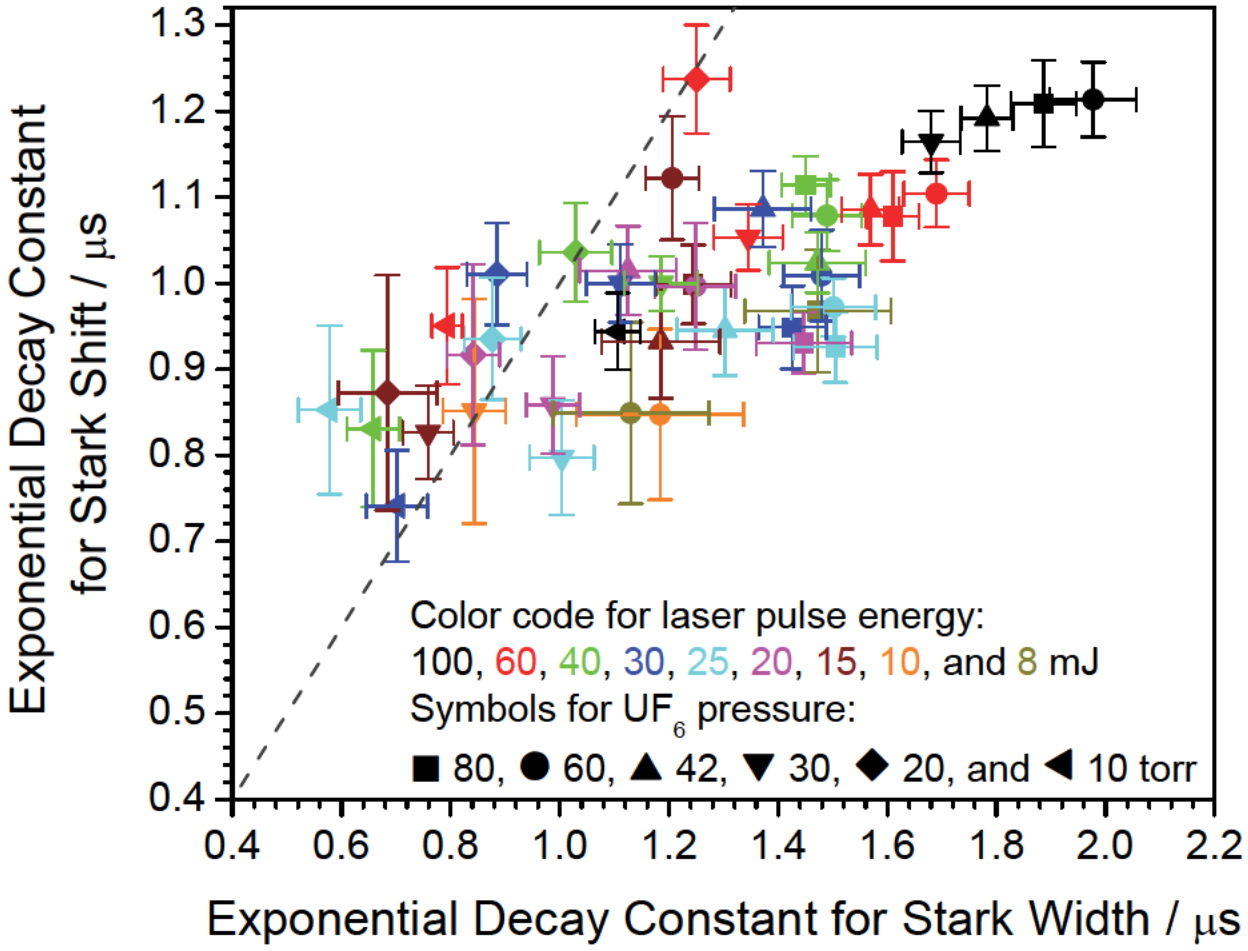
Exponential Decay Constant for Stark Shift / μs
Exponential Decay Constant for Stark Width / μs
1.3
1.2
1.1
1.0
0.9
0.8
0.7
0.6
0.5
0.4
0.4
0.6
0.8
1.0
1.2
1.4
1.6
1.8
2.0
2.2
Color code for laser pulse energy:
100, 60, 40, 30, 25, 20, 15, 10, and 8 mJ
Symbols for UF6 pressure:
■ 80, ● 60, ▲ 42, ▼ 30, ◆ 20, and ◀ 10 torr

Figure 7b

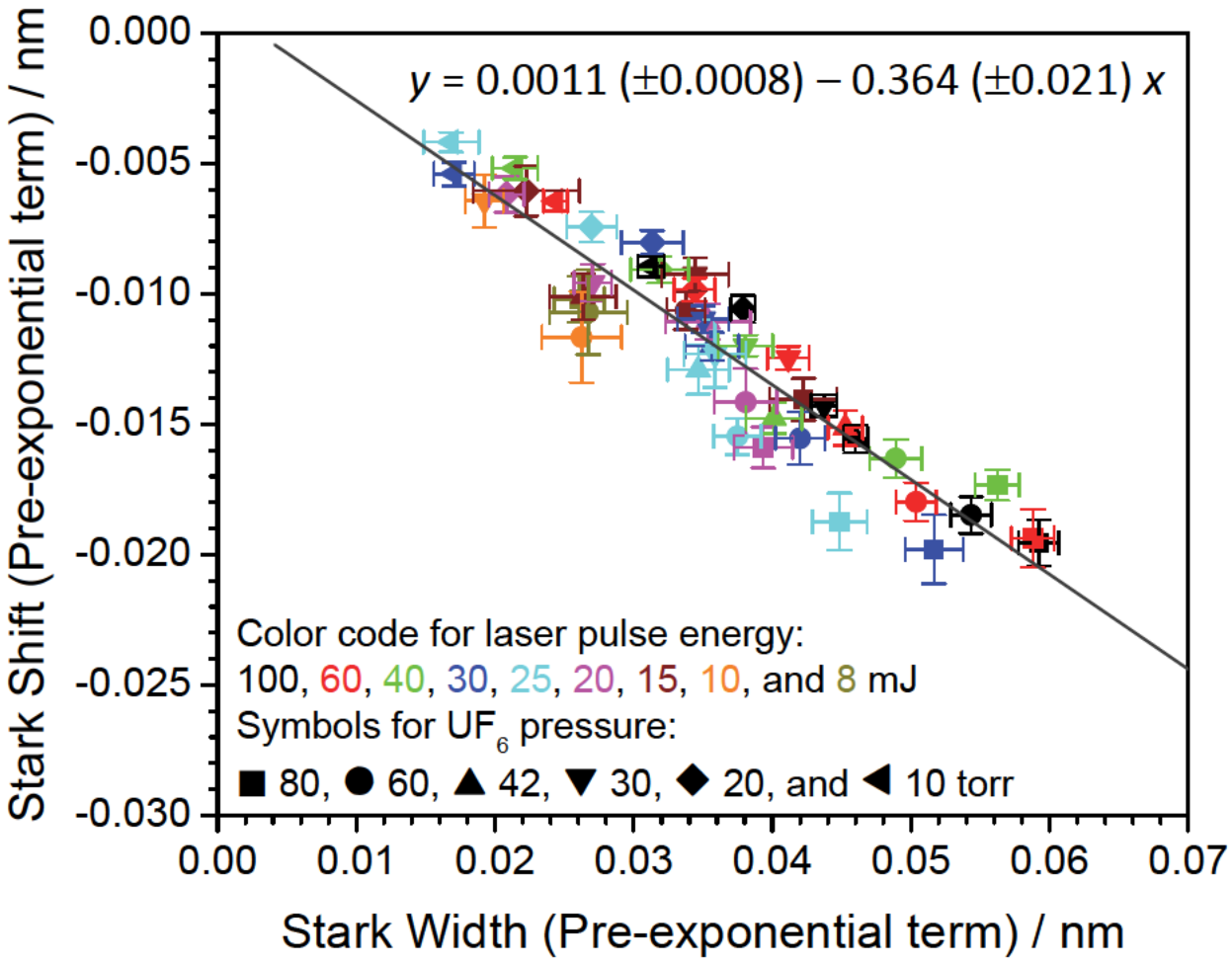
y = 0.0011 (±0.0008) – 0.364 (±0.021) x
Color code for laser pulse energy:
100, 60, 40, 30, 25, 20, 15, 10, and 8 mJ
Symbols for UF6 pressure:
■ 80, ● 60, ▲ 42, ▼ 30, ◆ 20, and ◀ 10 torr
Stark Shift (Pre-exponential term) / nm
0.000
-0.005
-0.010
-0.015
-0.020
-0.025
-0.030
0.00
0.01
0.02
0.03
0.04
0.05
0.06
0.07
Stark Width (Pre-exponential term) / nm

Figure 8a

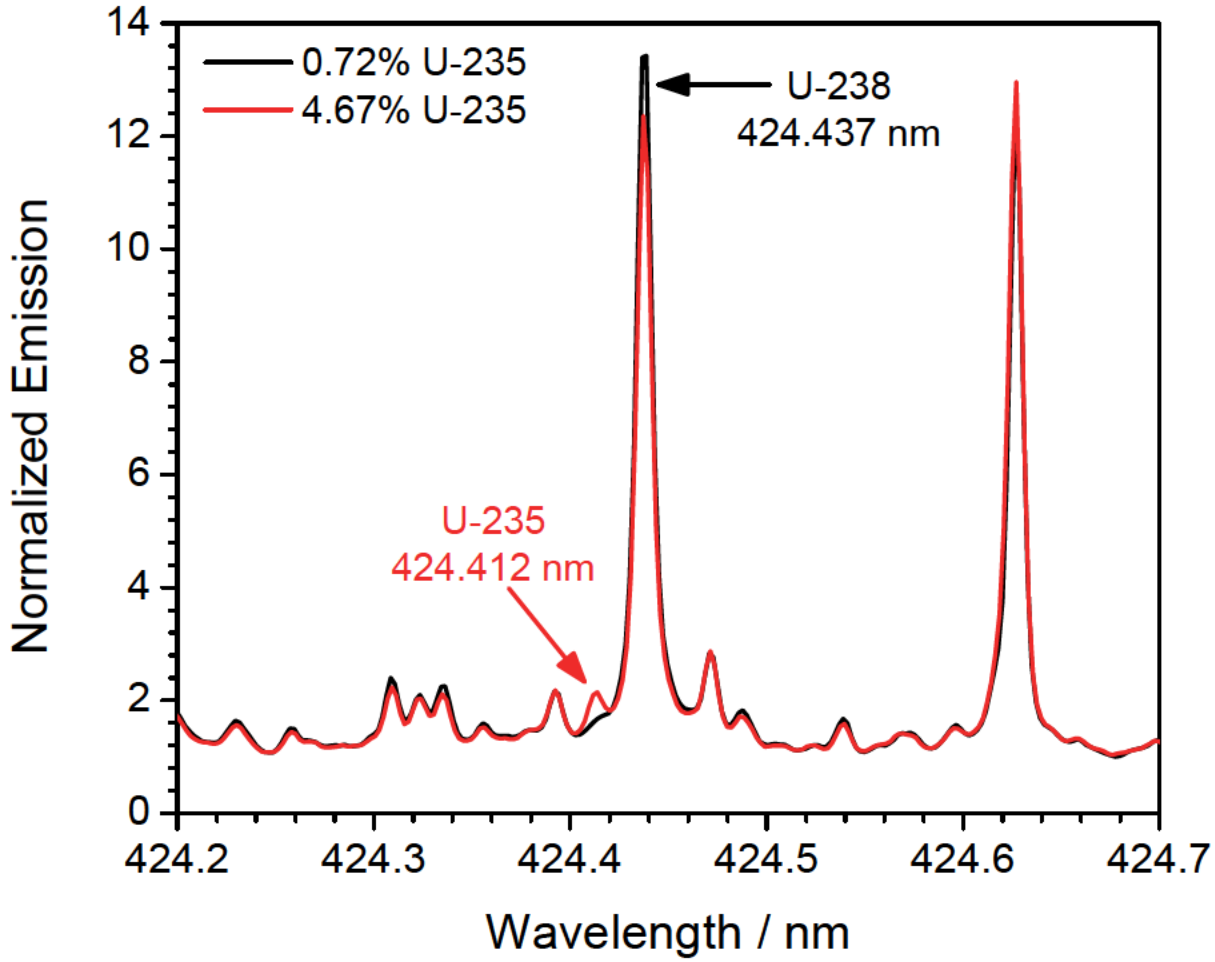

20190312, 6 torr, 30 mJ

Figure 8b

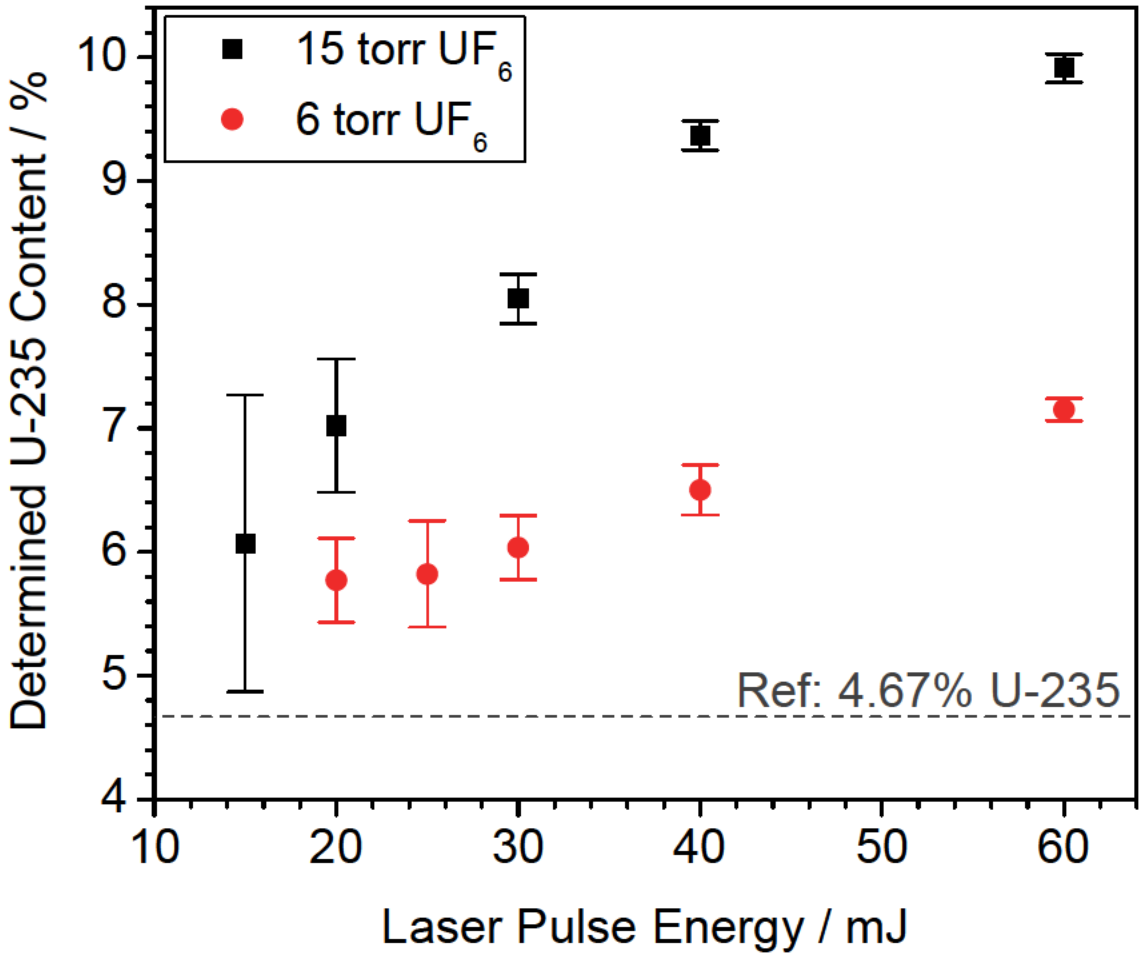
15 torr UF6
6 torr UF6
Ref: 4.67% U-235
Determined U-235 Content / %
Laser Pulse Energy / mJ
10
9
8
7
6
5
4
10
20
30
40
50
60

Figure 8c

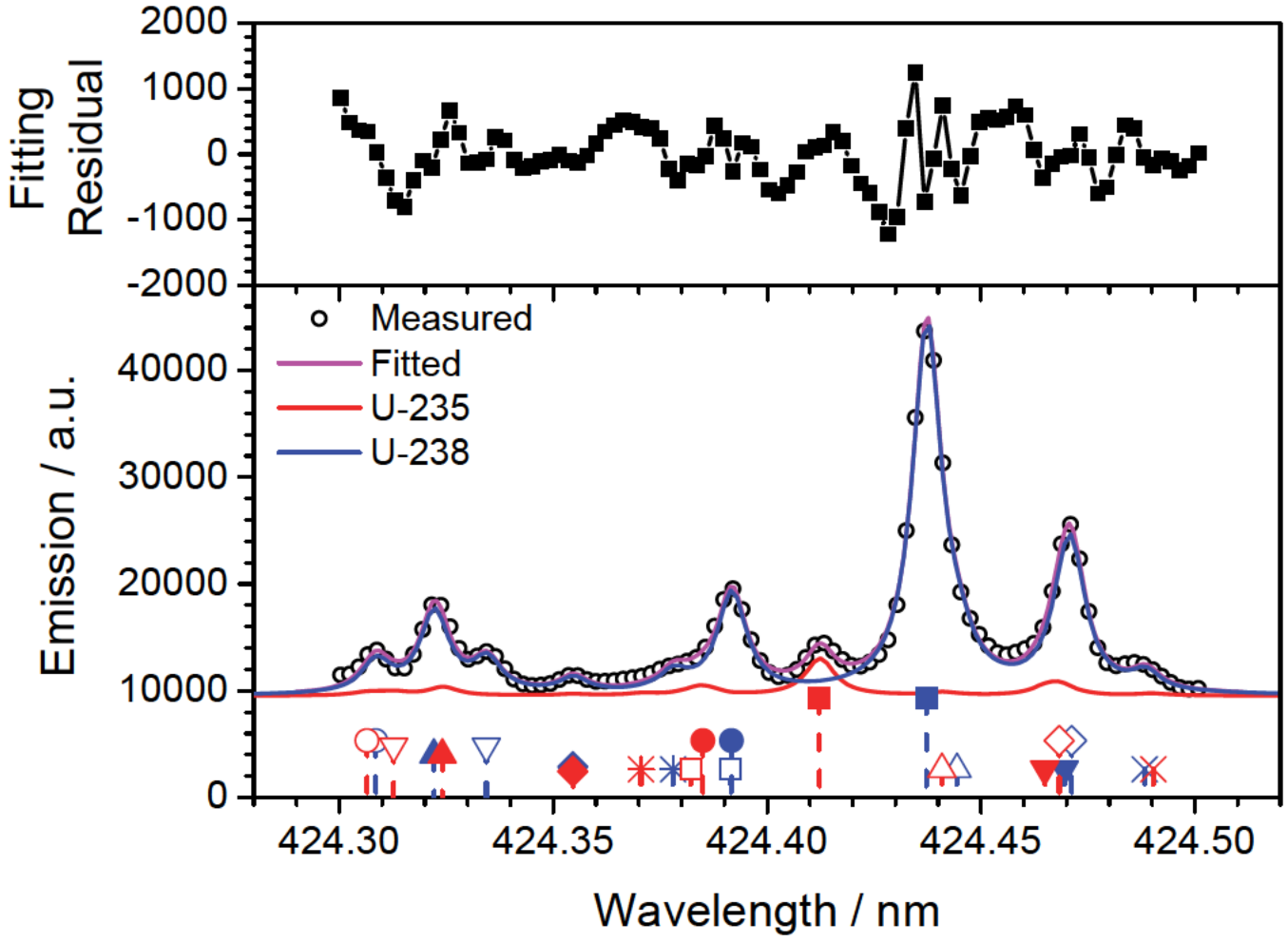

40 mJ, 15 torr

Figure 9a

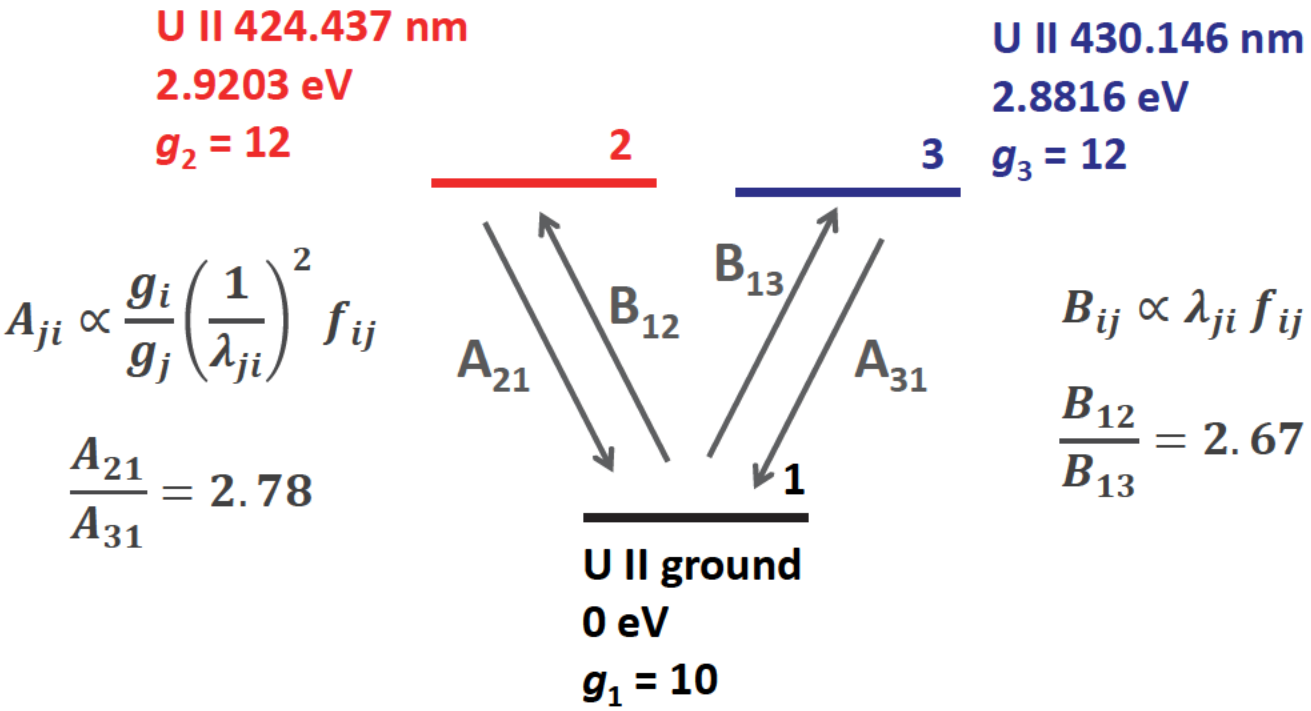
U II 424.437 nm
2.9203 eV
g_2 = 12
2
3
U II 430.146 nm
2.8816 eV
g_3 = 12
$A_{ji} \propto \frac{g_i}{g_j}\left(\frac{1}{\lambda_{ji}}\right)^2 f_{ij}$
$B_{ij} \propto \lambda_{ji} f_{ij}$
$\frac{A_{21}}{A_{31}} = 2.78$
$\frac{B_{12}}{B_{13}} = 2.67$
A21
B12
B13
A31
1
U II ground
0 eV
g_1 = 10

Figure 9b

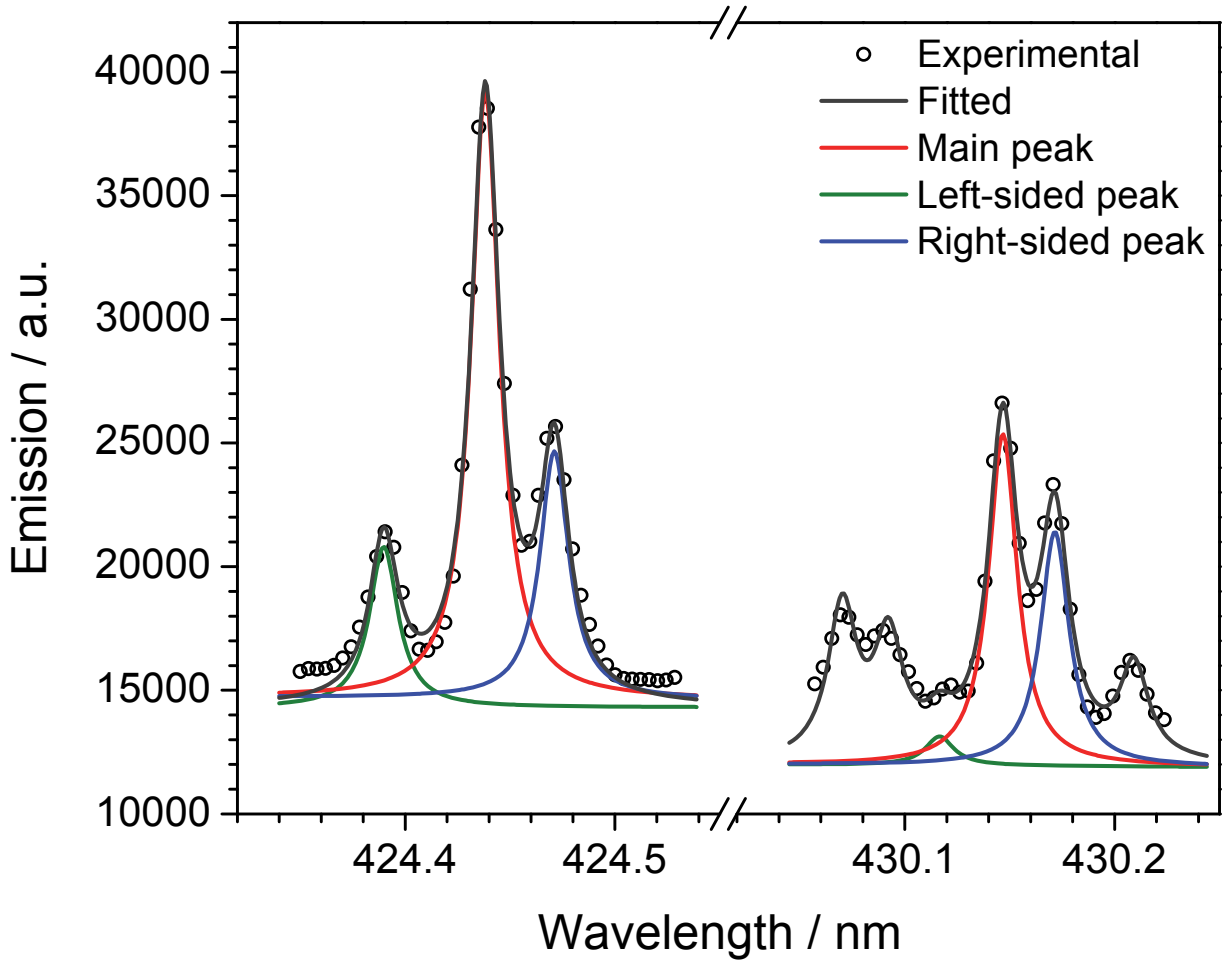

30 mJ

Figure 9c

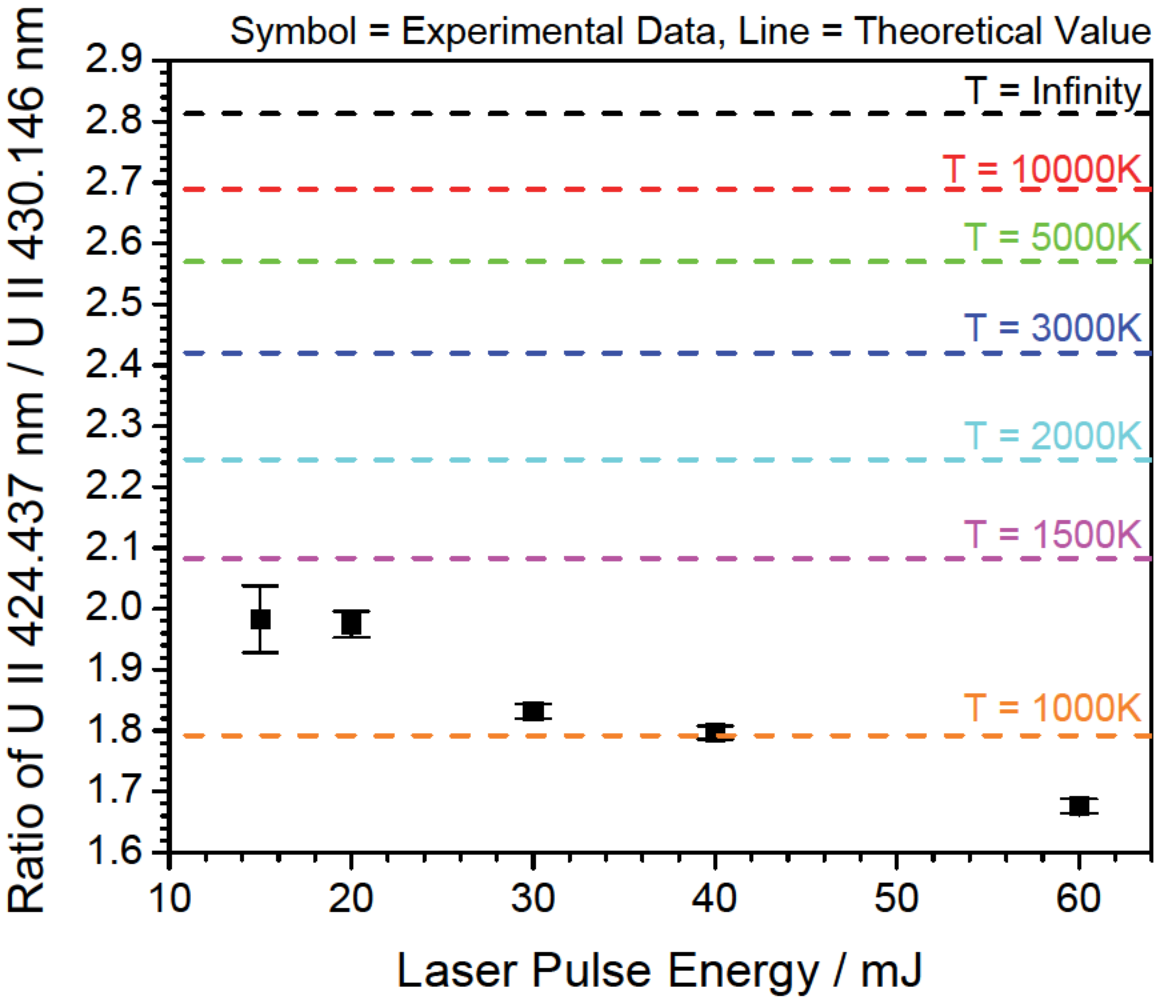
Symbol = Experimental Data, Line = Theoretical Value
T = Infinity
T = 10000K
T = 5000K
T = 3000K
T = 2000K
T = 1500K
T = 1000K
Ratio of U II 424.437 nm / U II 430.146 nm
Laser Pulse Energy / mJ
2.9
2.8
2.7
2.6
2.5
2.4
2.3
2.2
2.1
2.0
1.9
1.8
1.7
1.6
10
20
30
40
50
60

Figure 10

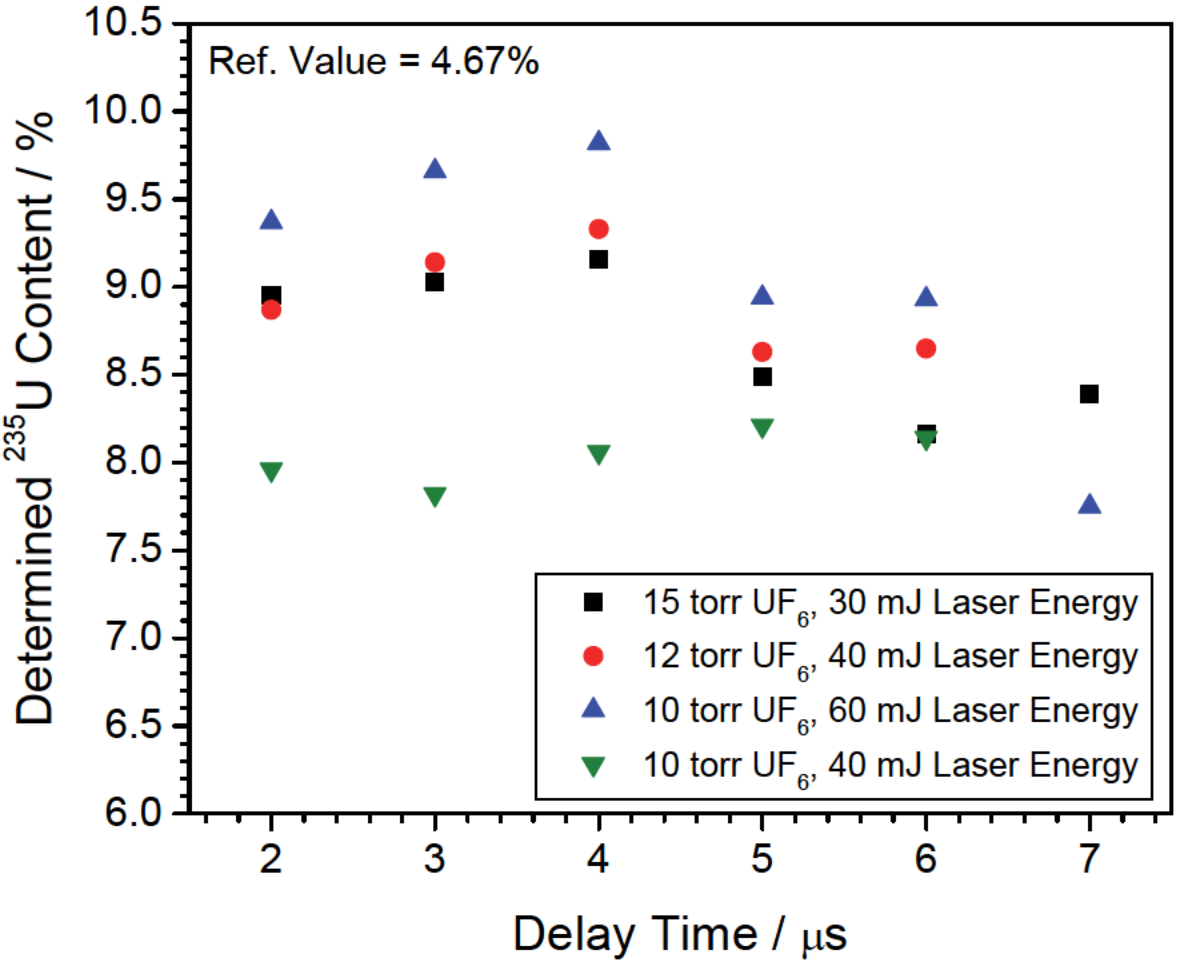
Ref. Value = 4.67%
Determined ^{235}U Content / %
Delay Time / μs
10.5
10.0
9.5
9.0
8.5
8.0
7.5
7.0
6.5
6.0
2
3
4
5
6
7
15 torr UF_6, 30 mJ Laser Energy
12 torr UF_6, 40 mJ Laser Energy
10 torr UF_6, 60 mJ Laser Energy
10 torr UF_6, 40 mJ Laser Energy